Experimental validation of the exact analytical solution to the steady periodic heat transfer problem in a PCM layer

Domenico Mazzeo[a,*], Giuseppe Oliveti[a], Alvaro de Gracia[b], Julia Coma[c], Aran Solé[d], Luisa F. Cabeza[e]

[a] Department of Mechanical, Energy and Management Engineering (DIMEG) - University of Calabria, P. Bucci 46/C - 87036 - Rende (CS) - Italy
[b] Departament d'Enginyeria Mecanica, Universitat Rovira i Virgili, Av. Països Catalans 26, 7 43007, Tarragona, Spain
[c] Departament Tecnologia de l'Arquitectura, Universitat Politècnica de Catalunya, Av Dr Marañon 44-50, 08028 Barcelona, Spain
[d] Department of Mechanical Engineering and Construction, Universitat Jaume I, Campus del Riu Sec s/n, 12071 Castelló de la Plana, Spain
[e] GREA Innovació Concurrent, INSPIRES Research Centre, University of Lleida, Pere de Cabrera s/n, 25001, Lleida, Spain

*Corresponding author. Domenico Mazzeo, email address: domenico.mazzeo@unical.it, tel.: +39 0984 494605, fax: +39 0984 494673

Abstract

Phase change materials (PCM) are used in many industrial and residential applications for their advantageous characteristic of high capacity of latent thermal storage by means of an isothermal process. In this context, it is very useful to have predictive mathematical models for the analysis of the thermal performance and the thermal design of these layers. In this work, an experimental validation of an analytical model that resolves the steady periodic heat transfer problem in a finite layer of PCM is presented. The experimental investigation was conducted employing a PCM with thermophysical and thermochemical behavior very close to those hypothesized in the formulation of the analytical model. For the evaluation of the thermophysical properties of the PCM sample used, an experimental procedure created by the authors was employed. In all tests realized in a sinusoidal and non-sinusoidal periodic regime, the comparison between the measured and calculated trends of the temperature at different sample heights and of the surface heat fluxes show an excellent agreement. Moreover, also having verified the analytical total stored energy, the analytical model constitutes a valid instrument for the evaluation of the latent and sensible contribution and the trend in time of the position of the bi-phase interface.

Keywords: PCM; Experimental validation; Analytical model; Thermophysical properties; New procedure; DSC.

1. Introduction

The use of phase change materials (PCM) is the object of increasing interest that has led to many applications in different contexts. Unlike traditional materials, PCM, owing to their solid-liquid phase change, allow the storage of a great quantity of latent energy at a constant temperature. For example, PCM are used in industrial plants for the storage of heating and cooling energy, in the air-conditioning of buildings to reduce energy in transit through the walls both in the summer season and in the winter season. PCM are also used in electronic equipment to ensure correct functioning, and in containers used for the transportation of food, drinks and medicines to prevent their deterioration [1]. In many of these applications, the thermal regime can be considered, with a good approximation, as steady periodic.

Several authors have addressed the problem of the thermal behavior of a PCM layer in steady periodic regime through analytical models, numerically solved, or through experimental investigations. The main researches concern the thermal behavior of plates and hollow cylinders in contact with a fluid [2-4], phase change storage system of solar energy [5-7] and multilayer building walls containing a PCM layer [8]. In the latter case, many studies regard the evaluation of the influence of PCM thermophysical properties and of the PCM thickness on the dynamic thermal characteristics [9-14] for different locations.

If on the one hand, a large number of numerical investigations in a steady periodic regime were addressed, only a small part of this research is supported by analytical or experimental validation. For instance, both in cylindrical [15] and plane [16-17] geometry are present studies that compare numerical results that describe the cyclical performance of a latent heat thermal storage system with experimental data. In the scientific literature, the experimental validation of an analytical model in a dimensionless form can be found, resolved with the finite volume method, for the study of the thermal behavior of a PCM layer with heat flux boundary conditions [18]. In another study, a set of experimental data was compared with the results of a numerical model considering cubical test cells subject to a sinusoidal external temperature evolution [19]. Savovic et al. [20] conducted a numerical study of the heat transfer in a PCM layer with a finite difference model in one-dimensional geometry with periodic boundary conditions. The evaluations of the position and velocity of the bi-phase interface and of the temperature fields were compared with those obtained with the Ozisik integral method [21]. Similarly, in the case of a PCM layer with a thin fin, a simplified numerical model that predicts the melt fraction and the form of the bi-phase interface as a

function of time was verified experimentally [22]. Finally, in the field of building physics the numerically evaluated thermal behavior of a building component with PCM was verified with experimental measurements.

For the analysis of the performance and the thermal design of such layers, the aforementioned studies highlight that it is extremely important to have experimentally validated predictive mathematical models. The use of these models requires the knowledge of the effective thermophysical properties of the layer, measurable with the most widespread experimental methods, namely DSC (Differential Scanning Calorimeter) technique developed by Watson et al. [25], and the T-History method proposed by Zhang et al. [26], or with new techniques [27, 28] proposed in trecent years.

Concerning the availability of predictive mathematical models, it is necessary to highlight that the problem of the determination of the temperature field in a layer subject to phase changes, known as the Stefan Problem, presents non-linear characteristics, which render the solving of differential equations describing the phenomenon particularly difficult. In particular, the domains of the differential equations are variable in time and are determined by the external surface boundary conditions as well as by the bi-phase interface conditions. These conditions are expressed by an instantaneous thermal balance equation, which describes conductive heat flux discontinuity, and by the constraint that at the bi-phase interface the temperature is equal to the phase change temperature. The thermal field in the two phases, which present different thermophysical properties, is a function of the position of the bi-phase interface that is variable in time as well as the relative boundary conditions.

The complexity of the problem has led many authors to use numerical procedures that implement simplified models to describe the phase change, such as the models known in the literature as latent-heat evolution methods [29]. The latter describe the movement of the bi-phase interface through different approaches known as the apparent heat capacity method, the effective heat capacity method, and the enthalpy method. Only a limited number of analytical solutions of the Stefan Problem are available and regard semi-infinite or finite layers with boundary conditions that are not variable in time [21, 29-34]. The analytical solutions present the advantage of identifying directly the physical parameters on which the thermal behavior of the system depends, and the function that connects the unknowns to the physical parameters and to the boundary conditions. Recently, in the laboratory of "Building Energy" of the Applied Physics Area of the Department of Mechanical, Energy and Management Engineering (DIMEG) at the University of Calabria, the exact solutions of

a Stefan Problem in a finite PCM layer in steady periodic regime was obtained [35]. The model allows for the determination of the bi-phase interface position, of the temperature and heat flux field, and of the energy stored in latent and sensible form.

The objective of this work is the experimental validation of such a model that was formulated supposing simplifying hypotheses regarding material behaviour and heat transfer in the layer as valid. Validation was made using a device developed by the GREA Innovació Concurrent research group at the University of Lleida (Lleida, Spain). This device contains two controlled chambers, heated and cooled by copper coils with thermos-stated water supplied by water baths, capable of setting different boundary conditions upon variation of time. Furthermore, it is equipped with a system for the measurement and acquisition of temperatures in the sample and of the surface heat fluxes. This equipment was used in a previous work to test the improvement in the thermal response of a gypsum board due to the incorporation of PCM [27]. For reduced heating/cooling rate values, the considered PCM presents, a melting temperature that is very close to the solidification temperature, a reduced phase change temperature range, and a slight difference between the latent heat of fusion and that of solidification. Moreover, the material neither present phenomena of phase segregation nor of subcooling. These properties are very close to those hypothesized in the formulation of the model. The thermophysical properties were determined by means of specific tests in the device conducted on the same PCM sample used for validation of the model. In this regard, a new experimental procedure has been developed, which is an advancement of the method used in de Gracia et al. [27]. The new procedure allows: (i) the evaluation of the thermophysical properties in the two phases; (ii) the obtainment of both the thermal conductivity and the specific heat with a sole experimental test; (iii) the evaluation of the latent heat and the phase change temperature. The results obtained were compared with those provided by the manufacturer and with those obtained in the laboratory by means of DSC tests. For the validation of the analytical model, different sinusoidal boundary conditions are considered, which give rise to reduced heating/cooling rates, obtained by varying the attenuation and the time lag between the two temperature loadings operating on the two boundary faces and the oscillation period. Moreover, the model was validated considering non-sinusoidal boundary conditions. Validation was made by comparing the measured and analytically calculated trends of the temperatures at different heights in the sample and of the surface heat fluxes, and by comparing the experimental total stored energy and that provided by the model.

In the first part of the paper, the authors present: (i) a description of the PCM employed and of the experimental device; (ii) the new procedure for the determination of the thermal conductivity and specific heat capacity in the two phases, latent heat and phase change temperature; (iii) a brief description of the analytical model for the determination of the position of the bi-phase interface and of the thermal field in the solid and liquid phases. Successively, the results of the new experimental procedure for the evaluation of the PCM thermophysical properties are described and compared with those provided by the manufacturer and with those obtained in the laboratory by means of DSC tests. Finally, the different experimental tests conducted in a steady periodic regime for validation of the analytical model are presented.

2. Materials and methodology

2.1. Experimental equipment

2.1.1. PCM description

The material considered in this study is the commercial PCM PureTemp23, provided by Entropy Solutions [36]. According to the manufacturer, the material presents consistent and repeatable performance over thousands of thermal (melt/solidify) cycles; it is 100% renewable, non-toxic and biodegradable since it is produced from natural agricultural sources (such as palm oil, palm kernel oil, rapeseed oil, coconut oil, and soybean oil). It does not undergo phase segregation and supercooling, the phenomenon in which a substance cools below its freezing point without solidifying.

The thermophysical properties and DSC curve of the Puretemp23 provided by the manufacturer, obtained with a heating rate of 1°C/min, are reported in Figure 1.

Figure 1 - PCM PureTemp23, thermophysical properties and DSC curve with a heating rate of 1°C/min [36].

2.1.2. Device for testing steady and dynamic response of a PCM layer

The experimental set-up used for the tests (Figure 2) is constituted of a wooden structure with external dimensions of 32 cm x 28 x 61 cm. All the exterior wooden panels (3 mm) are insulated with 3.5 cm of vacuum panels (thermal resistance = 0.14 $m^2 \cdot K/W$) and 2 cm of Pyrogel (k = 0.013

W/m K). The internal volume of the structure is divided into two separate air cavities (upper and lower) by a sample holder made of XPS insulation (19 x 19 x 8 cm). A cylindrical hole with dimensions of Ø 75 × 75 mm and two heat-flux meters located on the bottom and top of the sample holder retain the PCM sample in both liquid and solid phases. The insulating layer allows the lateral surface of the cylinder to be almost adiabatic and obtain a unidirectional heat flux in the axial direction. The two air cavities constitute controlled environments, heated or cooled by means of copper coils connected to two programmable water baths able to simulate different thermal conditions ranging from -10 ºC to 140 ºC. The temperature of each bath is regulated by hot or cold water flows produced in an individual heater/cooler system. This experimental equipment was developed at GREA Innovació Concurrent, University of Lleida (Spain) and was used by de Gracia et al. [27] in an earlier work to evaluate the improvement in the thermal behaviour by impregnating a PCM in a conventional gypsum board.

Figure 2 - Sections of the test-box scheme design.

The measurement of the heat flux on the two faces of the cylindrical sample of PCM is obtained by two heat flux meters (Hukseflux HFP01) with a diameter of 7.5 cm with an accuracy of ±5%. These two heat flux meters allow testing for one-dimensional heat transfer. In these conditions, the steady component (mean value) of the periodic heat flux on the upper surface is equal to that on the bottom surface. The temperature in the sample is measured using Ø 0.5 mm thermocouples type T, with an error of ±0.5 °C, in correspondence with the axis on the upper face (top point) and lower (bot point), and within the layer at 3 different heights (points 2, 3 and 4). The location of the previously introduced sensors is shown in Figure 3. A data logger acquires and registers the measured thermal quantity every 10 seconds.

The surface heat fluxes and the temperatures along the axis of the sample are used for the thermal analysis in a steady regime and in a transient regime for the evaluation of the thermophysical properties of the PCM, and in a steady periodic regime for validation of the analytical model.

Figure 3 - Position of the thermocouples TC and the heat flux meters HFM in the cylindrical PCM sample.

2.2. Determination of the PCM thermophysical properties

In this study two techniques are used to determine the thermophysical properties of the PCM: the DSC and a new procedure proposed by the authors.

In the first case a sample with reduced dimensions (10-50 mg) is employed, while in the second case experimental tests were conducted on the same sample used for validation of the model, which has notably greater dimensions (234 g). As reported in Cheng et al. [28], the thermophysical properties could be determined by the sample mass. For this reason, such tests are necessary to compare the thermophysical properties obtained by means of the procedure, with those provided by the manufacturer and those obtained with the DSC characterization.

2.2.1. DSC characterization

The DSC technique has been widely used to determine the thermophysical properties of different PCM [37, 38] and allows the evaluation of the stored heat trend per time unit and per mass unit upon temperature variation. In this study, the DSC is used for two purposes. The first experiments were designed to investigate the variability of the phase change temperature and of the latent heat (J/kg) upon variation of the heating/cooling rate. In this case, three dynamic tests were conducted at 0.5 K/min, 5 K/min, and 10 K/min. The second experiments were designed to determine the specific heat capacity *c* at different temperatures in the liquid and solid phase. The methodology to determine the specific heat capacity follows the one published by Ferrer et al. [39].
A Mettler Toledo DSC 822e was used to perform all the experiments. Two samples of the selected PCM for each experiment were tested under the same conditions to ensure repeatability of the results. The samples were placed in 40µl closed aluminium crucibles under 200 ml/min N_2 flow. Each sample mass was around 12 mg weighed in a Mettler Toledo AG135 analytical balance with a precision of 0.01 mg.

2.2.2. New procedure

Thermal conductivity and specific heat

Two tests were conducted for the determination of the thermal conductivity and of the specific heat. One test was conducted with the sample entirely in a solid phase and the other with the sample entirely in a liquid phase. The test consists of subjecting the sample to a thermal transient from an initial steady thermal state to a final steady thermal state without allowing the phase change to occur. The temperature and heat flux trends measured on the two faces during the thermal transient regime are used to evaluate the specific heat, while the values corresponding to the final steady

regime are used for calculation of thermal conductivity. Figure 4 shows a sketch of the temperature and heat flux trends on the two faces.

Figure 4 - Schematization of temperature trends T_{top} and T_{bot}, on the left, and of surface heat fluxes trends F_{top} and F_{bot} and of the stored sensible energy E_S, on the right, during the thermal transient between an initial steady state and a final steady state, to be used for the determination of the thermal conductivity and specific heat in the two phases.

The thermal conductivity is obtained using the measurement of the heat flux F_f and that of the temperatures $T_{top,f}$ and $T_{bot,f}$ on the two faces of the sample with the relation:

$$\lambda = \frac{F_f}{\left(T_{top,f} - T_{bot,f}\right)} L \qquad \text{(Eq. 1)}$$

The thermal conductivity of the solid phase and the liquid phase may also be determined, with a lower accuracy, using the thermal transient of the experimental tests by means of the progressive mean method [40].

The energy balance relating to the thermal transient between the initial instant t_0, with a linear temperature profile in the sample $T_0(x)$, and the final instant t_f, with a linear temperature profile in the sample $T_f(x)$, is expressed by the relation:

$$E_S = A \int_{t_0}^{t_f} \left(F_{top}(t) - F_{bot}(t)\right) dt = A\rho c \int_0^L \left[T_f(x) - T_0(x)\right] dx \qquad \text{(Eq. 2)}$$

The resolution of the preceding equation for the specific heat provides the relation:

$$c = \frac{A \int_{t_0}^{t_f} \left(F_{top}(t) - F_{bot}(t)\right) dt}{m\left[\left(\frac{T_{top,0} + T_{bot,0}}{2}\right) - \left(\frac{T_{top,f} + T_{bot,f}}{2}\right)\right]} \qquad \text{(Eq. 3)}$$

The procedure created represents an advancement of the method used in de Gracia et al. [27] in that it allows for differentiation of the thermophysical properties in the two phases and also allows the obtainment of both the thermal conductivity and specific heat with one experimental test.

Heat latent of fusion and phase change temperature

The experimental device was also used to determine the latent heat and the melting temperature. The tests conducted consist of a thermal transient with a solid-liquid phase change in the entire sample. The initial state is steady with a uniform temperature and the sample is in a solid phase, and the final state is also steady and the sample entirely in a liquid phase. Since the phase change at the different heights of the PCM sample starts and ends in different time instants, the energy balance of the sample was obtained as the sum of the energetic balance of the subvolumes associated with the single thermocouples. With reference to Figure 5, if t_0 and t_f are the initial and final instant of the thermal transient, the total energy stored by generic subvolume j of thickness Δx_j, expressed by the integral of the difference between the entering and exiting heat flux, is given by the sum: (i) of the sensible energy stored in the time intervals in which the subvolume is in the solid phase, between the instant t_0 and $t_{1,j}$, and in liquid phase, between $t_{2,j}$ and t_f; (ii) of the stored latent energy due to the phase change in the subvolume, in the interval ($t_{1,j}$, $t_{2,j}$). The sensible energy stored during the solid phase and during the liquid phase is obtained using the respective initial and final temperatures, while the latent energy stored is that corresponding to the phase change of the mass of subvolume m_j.

Figure 5 - Schematization of the temperature trend in a j-th node, on the left, and of the surface heat fluxes trends F_{top} and F_{bot} and of the total stored energy E_T, on the right, during the thermal transient between an initial steady state and a final steady state, to be used for the determination of the latent heat and of the phase change temperature.

For the entire sample, the total stored energy is obtained by summing the contributions of the n subvolumes:

$$A\sum_{j=1}^{n}\int_{t_0}^{t_f}\left[F(x_j-\Delta x_j/2,t)-F(x_j+\Delta x_j/2,t)\right]dt = \sum_{j=1}^{n}\left\{\rho_s c_{p_s} A\int_{x_j-\Delta x_j/2}^{x_j+\Delta x_j/2}\left[T_j(t_{1,j})-T_j(t_0)\right]dx\right\}+\sum_{j=1}^{n}\{m_j H\}+ +\sum_{j=1}^{n}\left\{\rho_l c_{p_l} A\int_{x_j-\Delta x_j/2}^{x_j+\Delta x_j/2}\left[T_j(t_f)-T_j(t_{2,j})\right]dx\right\} \quad \text{(Eq. 4)}$$

Developing the summation at the first member, for the total stored energy E_T the expression is obtained:

$$A\sum_{j=1}^{n}\int_{t_0}^{t_f}\left[F(x_j-\Delta x_j/2,t)-F(x_j+\Delta x_j/2,t)\right]dt = A\int_{t_0}^{t_f}\left[F_{top}(t)-F_{bot}(t)\right]dt = E_T \quad (Eq.\,5)$$

In the second member of Eq. 4, the first term represents the sensible energy stored in the solid phase $E_{S,s}$, the second term represents the stored latent energy E_L and the third term represents the sensible energy stored in the liquid phase $E_{S,l}$. Finally, resolving Eq. 4 for the latent heat H, the following relation is obtained:

$$H = \frac{\left(E_T - E_{S,s} - E_{S,l}\right)}{m} \quad (Eq.\,6)$$

As regards the determination of the phase change temperature, for each subvolume, the temperature value in the interval ($t_{1,j}$, $t_{2,j}$), corresponding to the phase change, was considered.

2.3. Analytical model

2.3.1. Description

The study of thermal exchange in a PCM, known as the Stefan or Moving Boundary Problem, subjected to steady periodic boundary conditions was developed in a previous paper [35] by simultaneously solving the general equation of conduction in the solid phase and in the liquid phase, coupled by bi-phase interface conditions and by boundary conditions on two faces. At the bi-phase interface, the difference in heat fluxes between the liquid phase and the solid phase is equal to the heat needed for the fusion/solidification process per unit time and the temperature is equal to the melting temperature. Interface conditions introduce complexity in the resolution of the temperature field given that the position of the bi-phase interface in various instants is unknown.

The Stefan Problem addressed regards a cyclic process, in a steady periodic regime, in which the two phases are active since the boundary conditions regard a temperature oscillation above the melting temperature on one face and a temperature oscillation below the melting temperature on the other face. In such conditions, in the layer, a sole bi-phase interface originates.

The model was determined supposing: (i) that the transfer of conductive heat is one-directional in the liquid phase, as well as in the solid phase; (ii) that the bi-phase interface is flat and the phase change is reversible and isothermal: hysteresis phenomena are excluded; (iii) the absence of

subcooling phenomena and of phase segregation; (iv) that the thermophysical properties of the PCM are constant with the temperature, but different in the solid and liquid phase; (v) that the difference of density between the solid phase and the liquid phase is negligible.

The temperature and heat flux fields and the bi-phase interface position are expressed through a Fourier series expansion. The steady thermal field and the fluctuating thermal field in the two phases are obtained separately. The analytical solution to such a Stefan problem is reported in synthetic form in Section 2.3.2, while the resolution procedure of the model and some applications of the solution are reported in detail in [35].

2.3.2. Constitutive equations of the analytical model

With reference to Figure 6-I, the equations of the model are:

- *General equation of conduction in phase (a) and in phase (b)*

$$\frac{\partial^2 T_a}{\partial x^2} - \frac{1}{\alpha_a}\frac{\partial T_a}{\partial t} = 0 \qquad 0 < x < X_M(t) \qquad\qquad \frac{\partial^2 T_b}{\partial x^2} - \frac{1}{\alpha_b}\frac{\partial T_b}{\partial t} = 0 \qquad X_M(t) < x < L \quad (Eq.\,7)$$

with $X_M(t)$ position of the bi-phase interface, T temperature at abscissa x and at time t, $\alpha = \lambda/(\rho c)$ thermal diffusivity, λ thermal conductivity, ρ density, c specific heat capacity and L thickness of the layer. Subscripts (a) and (b) indicate the two phases.

- *Stefan conditions at the bi-phase interface:*

$$\left[\lambda_a \frac{\partial T_a}{\partial x} - \lambda_b \frac{\partial T_b}{\partial x}\right]_{x=X_M} = \rho H \frac{dX_M}{dt} \qquad (Eq.\,8)$$

$$T_a(X_M, t) = T_b(X_M, t) = T_M \qquad (Eq.\,9)$$

In Eq. 8, H is the latent heat of fusion (J/kg) and dX_M/dt the advancement velocity of the bi-phase interface at the melting temperature T_M.

The periodic boundary conditions in terms of temperature on face *1* of abscissa x = 0 of layer *(a)* and on face *2* of abscissa x = L of layer *(b)*, using the harmonic method are:

$$T_a(0,t) = T_1(t) = \bar{\vartheta}_1 + \vartheta_1(t) = \bar{\vartheta}_1 + \sum_{k=1}^{n} \tilde{\vartheta}_{1_k}(t) \quad \text{(Eq. 10)}$$

$$T_b(L,t) = T_2(t) = \bar{\vartheta}_2 + \vartheta_2(t) = \bar{\vartheta}_2 + \sum_{k=1}^{n} \tilde{\vartheta}_{2_k}(t) \quad \text{(Eq. 11)}$$

with $\bar{\vartheta}$ temperature steady component, $\vartheta(t)$ fluctuation of null mean value, k order and n number of harmonics $\tilde{\vartheta}_k(t)$.

In these conditions, the thermal field in the layer is steady periodic and is placed in the form:

$$T(x,t) = \bar{\vartheta}(x) + \vartheta(x,t) = \bar{\vartheta}(x) + \sum_{k=1}^{n} \tilde{\vartheta}_k(x,t) = \bar{\vartheta} + \sum_{k=1}^{n} |\tilde{\vartheta}_k| \text{sen}(k\omega t + \varphi_k) \quad \text{(Eq. 12)}$$

$$F(x,t) = \bar{\phi} + \phi(x,t) = \bar{\phi} + \sum_{k=1}^{n} \tilde{\phi}_k(x,t) = \bar{\phi} + \sum_{k=1}^{n} |\tilde{\phi}_k| \text{sen}(k\omega t + \psi_k) \quad \text{(Eq. 13)}$$

with $\bar{\vartheta}(x)$ and $\bar{\phi}$ respectively steady component of the temperature at abscissa x and steady component of the heat flux, $\vartheta(x,t)$ and $\phi(x,t)$ fluctuations of the null mean value at abscissa x and time t, $\tilde{\vartheta}_k(x,t)$ and $\tilde{\phi}_k(x,t)$ sinusoidal components with amplitude $|\tilde{\vartheta}_k|$ and $|\tilde{\phi}_k|$, argument φ_k and ψ_k, and pulsation $k\omega$.

The bi-phase interface also presents a periodic trend:

$$X_M(t) = \bar{\chi}_M + \chi_M(t) = \bar{\chi}_M + \sum_{k=1}^{n} \tilde{\chi}_{M_k}(t) = \bar{\chi}_M + \sum_{k=1}^{n} |\tilde{\chi}_{M_k}| \text{sen}(k\omega t + \zeta_k) \quad \text{(Eq. 14)}$$

with $\bar{\chi}_M$ steady component of the bi-phase interface around which oscillates fluctuation $\chi_M(t)$, expressed as the sum of n harmonics $\tilde{\chi}_{M_k}(t)$ of amplitude $|\tilde{\chi}_{M_k}|$ and of argument ζ_k.

The steady contribution of the solution is obtained by resolving the conduction equation in the solid phase and in the liquid phase with the bi-phase interface at the melting temperature T_M of abscissa $\bar{\chi}_M$, not depending on time, and steady boundary conditions $\bar{\vartheta}_1$ and $\bar{\vartheta}_2$.

Figure 6 - Reference system of the bi-phase interface position, boundary conditions and temperature trend in the liquid phase (a) and in the solid phase (b) in the PCM layer. (I) steady component + oscillating component; (II) steady component; (III) oscillating component.

The resolution of the oscillating thermal field, with reference to a generic harmonic, is obtained with the phasors method [41]. Each generic harmonic $\tilde{\vartheta}_k$, $\tilde{\phi}_k$, $\tilde{\chi}_{M_k}$ of pulsation kω, is represented by means of the imaginary part of the relative phasor written in the complex form. For the temperature:

$$\hat{\vartheta}_k = |\hat{\vartheta}_k|[\cos(k\omega t + \varphi_k) + j\,\mathrm{sen}(k\omega t + \varphi_k)] = |\hat{\vartheta}_k| e^{j\varphi_k} e^{jk\omega t} \qquad \text{(Eq. 15)}$$

with $|\hat{\vartheta}_k| = |\tilde{\vartheta}_k|$ and $\arg(\hat{\vartheta}_k) = \arg(\tilde{\vartheta}_k)$.

Table 1 reports the resolutive equations of the steady model, with reference to Figure 6-II, and of the oscillating model, with reference to Figure 6-III. In particular, the table contains: (i) the equation of the heat conduction in the liquid phase and in the solid phase; (ii) the Stefan conditions at the bi-phase interface; (iii) the boundary conditions on the two external faces that delimit the layer.

Table 1 - Constitutive equations of the steady model and of the oscillating model.

In the table, the spatial coordinate in the reference system of the steady model is indicated with *x,* with origin on face 1, while in that of the oscillating model, it is indicated with x^*, with origin in correspondence of the steady component of the position of the bi-phase interface. The two coordinates are bound by the relation $x^* = x - \bar{\chi}_M$. The total temperature and heat flux field, with reference to a single harmonic, are obtained respectively with the relations:

$$T(x,t) = \bar{\vartheta}(x) + \tilde{\vartheta}(x - \bar{\chi}_M, t)$$
$$F(x,t) = \bar{\phi} + \tilde{\phi}(x - \bar{\chi}_M, t) \qquad \text{(Eq. 16)}$$

in which the oscillating component is reported in the reference system of the steady component.

The steady thermal field is that in a slab with two layers, one in solid phase and the other in liquid phase, with temperature $\bar{\vartheta}_1$ and $\bar{\vartheta}_2$ assigned on the two faces of the boundary, and with thicknesses defined by the steady component of the bi-phase interface.

For the oscillating thermal field, the use of the phasors method allows transformation of the partial differential equation, which describes heat conduction in the solid phase and in the liquid phase and the discontinuity of the heat flux at the bi-phase interface, in ordinary differential equations.

Substituting the boundary conditions in the general solution of the ordinary differential equations that describe heat conduction in the two phases, a system of algebraic equations is obtained. The resolution of this system provides the phasor associated with the oscillating component of the position of the bi-phase interface, which is successively used to determine the phasors associated with the thermal field.

Table 2 reports the solution to the steady model and to the oscillating model. The steady solution defines the position of the bi-phase interface $\bar{\chi}_M$ (Eq. 27), the temperature field in the two phases $\bar{\vartheta}_a(x)$ and $\bar{\vartheta}_b(x)$ (Eqs. 28 and 29), and the transferred heat flux $\bar{\phi}_a = \bar{\phi}_b = \bar{\phi}$ (Eq. 30). The oscillating solution is represented: by the equation for the determination of the phasor associated with the oscillating component of the bi-phase interface $\hat{\chi}_M$ (Eq. 31); by the phasors, function of the phasor $\hat{\chi}_M$, associated with the oscillating temperature $\hat{\vartheta}_a(x^*)$, $\hat{\vartheta}_{ab}(x^*)$ and $\hat{\vartheta}_b(x^*)$ (Eqs. 32, 33 and 34) and oscillating heat flux $\hat{\phi}_a(x^*)$, $\hat{\phi}_{ab}(x^*)$ and $\hat{\phi}_b(x^*)$ (Eqs. 35, 36 and 37), calculated in the two phases and in the portion of the layer subject to phase change. The equation for the determination of $\hat{\chi}_M$ is an implicit transcendental equation with complex parameters and unknowns, the solution to which cannot be expressed in symbolic explicit form. However, it is possible to determine it by means of dedicated algorithms once the parameter values are known. A parametric study and an analytical approximation of Eq. (31) were presented in a recent research by Mazzeo and Oliveti [42]. The oscillating components in the time domain are obtained successively considering only the imaginary part of the preceding phasors expressed in trigonometrical form.

Table 2 - Solution of the steady model and of the oscillating model.

In the table with $\gamma_a = (1+j)(\omega/2\alpha_a)^{1/2}$ and $\gamma_b = (1+j)(\omega/2\alpha_b)^{1/2}$ the propagation constants in the two phases are indicated.

The advancement velocity of the bi-phase interface $\tilde{\upsilon}_M$ is obtained deriving the oscillating component of the bi-phase interface:

$$\tilde{\upsilon}_M = \frac{d\tilde{\chi}_M}{dt} = \mathrm{Im}\left[j\omega\hat{\chi}_M e^{j\omega t}\right] = \omega|\hat{\chi}_M|\cos(\omega t + \zeta) \qquad \text{(Eq. 38)}$$

Substituting Eq. (38) in Eq. (8), the expression of the latent heat stored/released per unit time is obtained:

$$\tilde{\phi}_H = \rho H \tilde{\upsilon}_M \qquad \text{(Eq. 39)}$$

3. Results and discussion

3.1. PCM sample employed in the experimental device

The cylindrical PCM sample in liquid phase used in the device has a mass of 234.1 g and a diameter of 7.1 cm (the reduction of the diameter is due to a double cylinder layer of impermeable film used in the sample holder to avoid the liquid leakage in the test box). The density of the liquid phase of sample resulted as being equal to 0.831 g/ml while that of the solid phase to 0.865 g/ml. After the phase change, it was found that the volume variation is contained and is always less than 5%. The density value provided in the solid phase by the manufacturer results as being 5% higher compared to the value measured. Considering the density value measured in the liquid phase, the height of the cylindrical sample results as being equal to 7.11 cm (the reduction of the height is due to the placement of the heat flux meters at the top and bottom of the sample holder). In order to ascertain the exact placement of the thermocouples within the sample along the axis at different heights, a test in steady state with the sample in the solid phase was conducted by setting two different temperature values on the upper and lower faces. Considering the top surface as origin of the reference system, the resultant placements of the thermocouples are $x_{TC2} = 1.73$ cm, $x_{TC3} = 3.03$ cm and $x_{TC4} = 4.99$ cm. Finally, it is necessary to take into account that the bath temperatures are different from the sample face temperatures, owing to the heat losses towards the external environment or the heat fluxes from the external environment at temperature T_{env} through: (i) the boundary surfaces of the bath; (ii) the surfaces of the conduits that supply the coils; (iii) the surfaces of the walls that delimit the two cavities of the test box.

3.2. Determination of the PCM thermophysical properties

3.2.1. DSC characterization

On one hand, Table 3 summarizes for different heating/cooling rates the experimental results for the two samples in terms of the latent heat of fusion H_{fus} and of solidification H_{sol}, of melting T_{fus} and of solidification T_{sol} temperature, and of melting temperature range ΔT_{fus} and solidification temperature range ΔT_{sol}. In addition, the table shows the arithmetic mean values and the standard deviation of the values obtained using the two samples.

Table 3 - Summary of the DSC results for the two samples of PureTemp23 at 0.5 K/min, 5 K/min and 10 K/min.

Latent heat and phase change temperature results of PureTemp 23 obtained by DSC are repeatable, presenting a standard deviation of less than 3.7 kJ/kg for the latent heat, less than 0.23 °C for the phase change temperature and less than 0.16 °C for the melting and solidification temperature ranges, in all the different analyses obtained when varying the heating/cooling rate. Moreover, no remarkable differences (< 3.4 ºC) between melting and solidification temperatures are observed when applying a heating rate of 0.5 K/min. Nonetheless, this temperature difference becomes significant when increasing the heating/cooling rate, reaching a difference of around 10 K between T_{fus} and T_{sol} in the case of 10 K/min. This could be due to the sample not achieving thermal equilibrium when applying high heating/cooling rates and also for the crystallization process. Analogously, the melting and the solidification temperature ranges are reduced respectively from 10.00 °C and 6.54 °C to 2.53 °C and 0.44 °C by reducing the heating/cooling rate from 10 K/min to 0.1 K/min. This behaviour upon variation of the heating/cooling rate is confirmed in other works available in the scientific literature [43-45]. It is noteworthy that the latent heat provided by the manufacturer, 201 J/g at 1 K/min (see Figure 1), is between the latent heat presented in this paper (see Table 3) at 0.5 and 5 K/min. On the contrary, this trend is not observed for the melting temperature, with a difference of 1.52 K and 1.89 K between the manufacturer value and the results presented here at 0.5 and 5 K/min, respectively.

In summary, in the case of PureTemp 23, upon diminishment of the heating/cooling rate, the melting temperature decreases, the solidification temperature increases and both the melting and the solidification temperature range reduce and become almost the same, while the latent heat of fusion is very close to that of solidification in all the different tests, and upon the decrease of the heating/cooling rate it undergoes a slight increase.

The analysis performed established that the experimental tests to be conducted for the validation of the analytical model should be performed at heating/cooling rates equal or lower than 0.5 K/min. This allows a reduced difference between the melting temperature and the solidification temperature to be obtained and the phase change temperature range to be contained.

On the other hand, Figure 7 shows the specific heat capacity *c* as a function of temperature. The specific heat capacity of PureTemp 23 is 1.55 (±0.01) kJ/kg·K at 10 ºC and 2.05 (±0.03) kJ/kg·K at 40 ºC. The results obtained with the two samples are in agreement, ensuring repeatability of the results. The manufacturer provides the specific heat capacity at both phases without specifying at which temperature they are measured. Nevertheless, if these results are compared, they are also in

agreement especially for the liquid phase, which presents a difference of 0.06 kJ/kg·K whereas for the solid phase it is 0.29 kJ/kg·K.

Figure 7 - Specific heat capacity as a function of the temperature for the solid phase and liquid phase of the two samples of Pure Temp 23.

3.2.2. New procedure

Thermal conductivity and specific heat

For the determination of the thermal conductivity and the specific heat in both solid and liquid phase the method described in Section 2.2.2 was applied. For the solid phase, starting from a uniform temperature of 0 °C in the sample, at the initial instant t_0 the temperature of the upper water bath was modified and set at 18°C. For the liquid phase, starting from a steady field in the sample at a constant temperature of 28.5 °C, at initial instant t_0, the temperature of the upper bath was modified and set at 90 °C.

The trends of temperatures at different heights and of the surface heat fluxes recorded during the thermal transient process are reported for the solid phase and for the liquid phase in Figure 8. The trends of the sensible energy stored per unit time, calculated as the difference between the surface heat fluxes, are reported in the figures showing the trends of the surface heat fluxes.

Figure 8 - Trends of the temperatures TC at different heights, of the surface heat fluxes HFM and of the sensible energy stored per unit time $E_{S,t}$. (a) and (b) solid phase; (c) and (d) liquid phase.

Figure 8 highlights that the thermal transient in the test, (a) and (b), with the sample in a solid phase has a duration of approximately 12 hours, while in the test with the sample in a liquid phase, (c) and (d), it has a duration of approximately 15 hours. The different duration is due to the different specific heat capacity in the two phases and to the different temperature excursion imposed at the initial time instant on the top surface.
In both tests the temperature trends and the bottom heat flux trend increase until becoming constant once the final steady state was reached. The top heat flux increases at the beginning, it successively reaches a maximum value and at the end decreases and becomes constant in correspondence to the final steady state.

Table 4 presents a summary of the values of the initial and final temperatures and of the final heat flux used for the calculation of the thermal conductivity and of the specific heat of the solid phase and the liquid phase, calculated with Eq. (1) and Eq. (3).

Table 4 - Measured values of temperatures T_{top} and T_{bot} on the two faces of the sample at final instant t_f and initial instant t_0 of the thermal transient, of steady heat fluxes F_f at final instant t_f, of the stored sensible energy E_S, of the thermal conductivity λ and of the specific heat capacity c, in the two experimental tests with the sample entirely in solid and in liquid phase.

The comparison between the thermal conductivity values provided by the manufacturer and those obtained by the experimental investigation show a deviation of -7.3% for the solid phase and +6.1% for the liquid phase. Instead, the thermal conductivity values obtained for the solid phase and for the liquid phase, employing the mean progressive method, resulted as being, respectively, 0.235 W/m K and 0.178 W/m K.

Regarding the specific heat, the results obtained were compared with those reported in Section 3.2.1, which highlight a dependence of the specific heat on the temperature. The values obtained in the experimental device correspond to an average temperature in the sample in the thermal transient equal to T_{sample} = 7.7 °C for the solid phase test and to T_{sample} = 44.5 °C for the liquid phase test. In correspondence to these temperatures, the curve of *c(T)*, shown in Figure 7, for the solid phase provides a value of $c_s = 1514.2\ (J/kg \cdot K)$ and for the liquid phase a value of $c_l = 2049.3\ (J/kg \cdot K)$.

Heat latent of fusion and phase change temperature

For the determination of the latent heat and of the phase change temperature, the method considered is described in Section 2.2.2. Starting from a steady field in the sample in solid phase at a uniform temperature equal to 15 °C, at initial instant t_0 the temperature of the upper water bath and that of the lower water bath were modified in order to obtain a uniform temperature equal to 29 °C at the end of the thermal transient in the sample.

Figure 9 respectively reports the temperature trends at the different heights and the trends of the surface heat fluxes recorded during the thermal transient. Figure 9b also reports the trend of the energy stored per unit time, sum of the sensible contribution and of the latent contribution.

Figure 9 highlights that the thermal transient has a duration of approximately 36 hours, proving the high latent storage capacity of the PCM. The solid-liquid phase change in the sample, owing to the

effect of the considered boundary conditions, initially occurs on the two boundary surfaces and then proceeds towards the inside until it determines the phase change in the entire volume.

Figure 9 – (a) Temperature trends at the different heights; (b) trends of the surface heat fluxes and of the sensible energy stored per unit time.

The recorded temperature trends show that the heating rate during the solid phase reduces proceeding from the two boundary faces *top* and *bo*t towards the inside of the sample, in correspondence with thermocouples TC3, TC4 and TC5. This reduction determines a decrease of the melting temperature proceeding towards the inside of the sample, as shown by the trends in Figure 9a during the phase change. In particular, the heating rate is 0.027 K/min on the top face, 0.022 K/min on the bot face, and 0.017 in correspondence with TC3, TC4 and TC5. The corresponding melting temperatures are approximately: 26.2 °C on the face top; 24.7 °C on the face bot; 22.47 °C for the three internal thermocouples. The dependence of the melting on the heating rate has already been highlighted with the DSC tests in Section 3.2.1.

In the experimental tests, conducted to verify the analytical model, the periodic trends of the temperatures made in the sample give rise to heating/cooling rates of between 0.001 and 0.01 K/min. For this reason, the phase change temperature used in the analytical model was assumed at 22.47 °C, with which is associated the lower heating rate, in correspondence with TC3, TC4 and TC5, in the experimental test.

Regarding the evaluation of the latent heat, Table 5 reports the sensible energy stored in the solid phase and in the liquid phase for each subvolume, represented respectively by the first and third term of the second member of Eq. 4, and the total energy stored in the entire sample, represented by the first member of Eq. 4.

Table 5 - Sensible energy stored in the solid phase and in the liquid phase by each subvolume and by the entire layer, total sensible energy stored and total energy stored.

Applying Eq. 6, taking into account the values in Table 5 and of the sample mass equal to m = 234.1 g, a value of H = 221.18 kJ/kg is obtained. This result confirms the slight increase undergone by the latent heat upon the decrease of the heating/cooling rate, as highlighted in Section 3.2.1.

3.3. Validation of the analytical model

Table 6 reports the thermophysical properties of the PCM sample used in the experimental device to verify the analytical model.

Table 6 - Thermophysical properties of the PureTemp23 PCM sample used in the device.

Regarding the density, since the model provides for an identical value in the two phases, the value ρ reported in the table is the average between the liquid phase density and the solid phase density.
The periodic temperature conditions on the two faces of the sample were set by the fluid temperatures in the two thermal baths. The resulting surface temperature were successively interpolated by a Fourier series expansion and used as the boundary conditions in the analytical model. The achievement of the validation of the analytical model with different boundary conditions requires the conduction of: (i) several tests in the sinusoidal periodic regime by varying the attenuation factor and the time lag between the temperature oscillations on the two faces, and the period of oscillations; (ii) one test in the non-sinusoidal periodic regime to consider the effect of multiple harmonics.
Table 7, both in the case of sinusoidal temperature boundary conditions and in the case of non-sinusoidal temperature boundary conditions, reports for each harmonics used in the Fourier series expansion: the order k and the period P, the mean steady value $\bar{\vartheta}_1$ and $\bar{\vartheta}_2$, the amplitude $|\tilde{\vartheta}_1|$ and $|\tilde{\vartheta}_2|$, and the argument $\arg(\tilde{\vartheta}_1)$ and $\arg(\tilde{\vartheta}_2)$ of the surface temperature loadings, the attenuation factor f and the time lag Δt between the two loadings.

Table 7 - Tests in a sinusoidal and non-sinusoidal regime: order k and period P of the harmonics used in the Fourier series expansion, mean steady value $|\tilde{\vartheta}_1|$ and $|\tilde{\vartheta}_2|$, amplitude $|\tilde{\vartheta}_1|$ and $|\tilde{\vartheta}_2|$, and argument $arg(\tilde{\vartheta}_1)$ and $arg(\tilde{\vartheta}_2)$ of the two boundary conditions, attenuation factor f and time lag Δt between the two boundary conditions.

In the different tests, the interpolation of the boundary conditions by the Fourier series expansion was obtained with correlation indexes R^2 very close to the unit. The same value in all the experiments was assigned to the mean value of the temperature of each fluid with the aim to obtain in the various tests the same mean temperature value on the top surface and the same temperature value on the bottom surface. The mean temperature measurements resulted as being equal, respectively, to 33.8 ± 0.8 °C and 12.5 ± 0.2 °C. Thus, the tests differ only in terms of the fluctuating component. Furthermore, the top surface temperature at each instant is greater than the

melting temperature, while the bottom surface temperature is always lower than the melting temperature. In these conditions, a sole bi-phase interface is achieved in the layer that divides the liquid phase, which is always placed in the upper part of the sample, from the solid phase, placed in the lower part of the sample.

TEST 1 is the reference test and regards boundary conditions that are both sinusoidal with a period of 24 hours. The amplitude and the argument of the temperature oscillation on the top face are, respectively, 9.547 °C and 0.950 rad, while on the bottom face the temperature oscillation is attenuated and undergoes a time lag, respectively, of 0.459 rad and 6.166 rad. In TEST 2 the boundary condition on the bottom face was modified, reducing the attenuation factor to 0.104. This modification gave rise to a slight variation of the time lag. In TEST 5 the boundary condition on the bottom face was modified to obtain a different time lag of 1.508 rad, which led to a slight modification of the attenuation factor. Only the period of the oscillations on the boundary surface of the sample was modified in TEST 4. An additional test to validate the analytical model in non-sinusoidal conditions was conducted. This experimental test regards a non-regular fluctuation with period equal to 24 hours on the top face and on the bottom face described through a Fourier series expansion truncated at the fifth harmonic.

In the different tests, the achievement of a steady periodic regime was held to be satisfied when in two successive cycles, the temperature trends at the different heights present mean deviations of less than 3% and those of the surface fluxes less than 5%. For example, in the case of TEST 1, Figure 10 reports the thermal transient evolution up to the reaching of the steady periodic regime of the temperatures at the different heights and of the surface heat fluxes. The regime conditions are achieved after four 24-hour cycles.

Figure 10 - Thermal transient during TEST 1 until attainment of the steady periodic regime of temperatures at different heights and of the surface heat fluxes.

Since the experimental device employed does not allow the direct measurement of the position of the bi-phase interface at each time instant, the experimental verification of the analytical model was obtained directly by comparing

- The temperature values measured and calculated at five different heights;

and indirectly by comparing

- The heat flux values measured and calculated on the two faces of the sample;

- The values of the total energy stored calculated with the analytical model and those obtained through the integral in time of the difference in the measured surface heat fluxes.

In the case of tests in a sinusoidal periodic regime, Figure 11 reports the comparison between the experimental temperature trends at different heights and of the surface heat fluxes, and the trends obtained analytically with the equations presented in Table 2. The analogue figures relative to the test in a non-sinusoidal periodic regime are reported in Figure 12. In the latter case, the analytical profiles were obtained by applying the equations relative to the steady model and, for the different harmonics, those relative to the oscillating model.

Figure 11 - Comparison between the measured (TC and HFM) and calculated (T and F) temperature trends at different heights, on the left, and of the surface heat fluxes, on the right, in the case of test in a sinusoidal periodic regime. From the top to the bottom in the order: TEST1, TEST2, TEST4 and TEST5.

Figure 12 - Comparison between the measured (TC and HFM) and calculated (T and F) temperature trends at different heights, on the left, and of the surface heat fluxes, on the right, in the case of test in a non-sinusoidal periodic regime.

The experimental temperature trends in all the tests confirm that for the boundary conditions considered, represented by trends TC1 and TC5, a sole one bi-phase interface is present in the layer. It remains highlighted in all the tests by the TC3 trends since they intersect the phase change temperature, and in tests 1, 2 and 5 also by the TC2 trends, which for a brief time interval reaches the phase change temperature while during the remaining part of the period it is in liquid phase.
The temperature fluctuations in the solid phase (TC4 and TC5) and in the liquid phase (TC1 and TC2), not involved in the phase change, present regular trends that attenuate and undergo a time lag proceeding from the two boundary surfaces towards the inside of the layer, in proximity to the portion involved in the phase change. In this portion, a smaller amplitude of the temperature fluctuation is recorded as the heat fluxes in transit in the two phases are converted into latent energy.

The qualitative comparison between the experimental trends and the trends calculated with the analytical model is, overall, very good in that in all the tests, since the periodic fluctuations present similar mean values, amplitudes and appear to be in phase. In particular, the deviations recorded on the temperature trends result as being very reduced in the portions of the layer that are always in liquid phase and in solid phase, while in the portion affected by the phase change, the deviations are more evident. Instead, regarding the measured heat flux, compared to that calculated with the

analytical model, on the top surface it presents a slightly lower amplitude, whereas on the bottom it has a slightly greater amplitude.

Such quantitative deviations recorded are to be attributed:

- to the non-one-directionality of the heat flux caused by:
  - The imperfect adiabaticity of the lateral boundary surface of the cylindrical sample. In particular, having recorded an external environment temperature close to the melting temperature in all the tests, the liquid phase of the sample transfers heat to the external environment while the solid phase receives heat from the external environment. This finds confirmation in the measured heat flux values, which on the bottom surface present a higher mean steady value and a higher amplitude compared to those calculated with the analytical model, while on the top surface they are lower (see Table 8 for the steady values and Figures 11 and 12 for the amplitudes).
  - The convective effects in the portion of the layer in liquid phase which increase the thermal losses towards the external environment. As proposed by other authors [16,18], addressing similar experimental tests, the convection phenomena can be neglected in a PCM layer with a small thickness.

  For each test, Table 8 reports the mean steady value of the heat flux measured on the top and bottom surfaces, the absolute and percentage deviation, the mean steady value of the analytically calculated heat flux and the percentage deviation between the two measured steady heat fluxes and the analytical one.

Table 8 - For the different tests, heat flux steady mean value measured on the top surface $\overline{HFM_{top}}$ and on the bottom surface $\overline{HFM_{bot}}$, absolute $\Delta_{\overline{HFM}}$ and percentage Δ% deviation, heat flux steady mean value calculated analytically $\bar{\phi}$ and percentage deviations Δ_{top}% and Δ_{bot}% between the two measured heat fluxes and the analytical one.

The table shows that, since the percentage deviations are in the order of ± 6%, and close to the error of measurement of the heat flux meters, in the experimental device the conditions of adiabaticity can be held to be sufficiently verified and that conduction plays the main role in the heat transfer in the layer. In such conditions, the heat transfer is almost one-dimensional.

- to the hysteresis phenomenon, a function of the heating/cooling rate, which gives rise to a melting temperature that is different from the solidification temperature, and to a melting latent heat that is slightly different from that of solidification; to the dependence of the phase change temperature range and of the latent heat on the heating/cooling rate. This

phenomenon greatly influences the temperature trends in proximity to the portion of the layer subject to phase change.

- to the variability of the specific heat in the liquid phase and in the solid phase with the temperature, as already shown in Figure 7, compared to the analytical model that uses the mean values in the two phases.
- to the slight difference in density in the two phases (±2% compared to the mean value), which in the analytical model is assumed as constant and equal to the mean value.
- to the slight variation of the volume following the transition phase, which produces a variation of the length of the sample of 4% in the case in which the entire layer changes phase. In the tests, only a reduced portion of the layer is subject to phase change.
- to the experimental trends produced by a steady periodic regime that are respected with an error always lower than 5%, and to the slight difference between the experimental and analytical boundary conditions, represented with a Fourier series expansion truncated at the fifth harmonic.

Despite the abovementioned experimentally detected phenomena, the basic hypotheses and the results of the analytical model result as being sufficiently verified. Therefore, the model can be used validly for the study of the dynamic thermal behaviour of a PCM layer and for the evaluation of stored energy in latent and sensible form. A further validation, in energy terms, of the predictive capacity of the model was obtained by comparing the total stored or released energy of the sample in the different experiments obtained with the analytical model. Table 9 shows the total stored energy determined experimentally and that calculated analytically as well as the percentage deviation.

Despite propagation of the error in the calculation of $E_{T,exp}$ as the integral of the difference between the two surface heat fluxes, measured with an accuracy of ± 5%, and the basic assumptions of the analytical model that have not been perfectly verified, the deviations are less than 8% in a periodic sinusoidal regime and of the order of 15% in a non-sinusoidal periodic regime.

Table 9 - For the different tests, experimental and analytical value of the total stored energy and percentage deviation.

Moreover, Table 9 shows that the maximum total energy stored is recorded in the case of TEST 1, with a higher attenuation factor and boundary conditions that are almost in phase. The reduction of the period gives rise to a reduction of the total stored energy.

The validated analytical model was used to determine the trend upon variation of the time of the bi-phase interface position. From the latter it was possible to evaluate the latent stored energy by means Eqs. (38-39) and then the sensible stored energy as the difference between the total and the latent stored energy. These results for the different tests are reported for the position of the bi-phase interface in Figure 13 and for the stored energy in Table 10.

Figure 13 - For the different tests, trend of the position of the bi-phase interface as a function of time.

In the different tests, the position of the bi-phase interface fluctuates within the layer between the abscissae x = 2.4 cm and x = 3.6 cm, determining a phase change of, at most, 17% of the thickness of the PCM layer.

Table 10 - For the different tests, sensible and latent stored energy.

The reduced value of the stored latent energy, compared to the sensible one, is due to the contained extension of the portion subject to phase change.

4. Conclusions

An experimental validation of an analytical model resolving the Stefan Problem in a PCM layer subjected to steady periodic boundary conditions that give rise to a sole bi-phase interface was conducted. The temperature boundary conditions considered regard sinusoidal and non-sinusoidal periodic trends. The model was verified by comparing the measured and calculated temperature trends at different heights in the layer, the trends of the surface heat fluxes, and the total stored energy. Thermophysical properties determined by means of experimental tests obtained using the same PCM test sample were used. To this end, a new procedure allowed for the determining of the thermal conductivity and of the specific heat in the liquid phase and in the solid phase, of the latent heat and of the phase change temperature with a limited number of tests in an experimental device. The values obtained are close to those provided by the manufacturer and those determined by DSC characterization.

The analytical model provides accurate predictive assessments as the temperature fluctuations throughout the layer and the surface heat flux fluctuations result as being very close to the experimental ones. In particular, the trends have similar mean values, of the amplitudes and of the

arguments. The deviations recorded on the temperature trends are significantly reduced in the portion of the layer that is always in a liquid phase and in a solid phase, while they are more evident in the portion involved in the phase change. As regards the measured heat flux, compared to that calculated with the analytical model, on the top surface it presents slightly higher amplitude, whereas on the bottom it has a slightly lower amplitude. These slight differences are mainly attributable to: the thermal field that is not strictly one-dimensional because of the imperfect adiabaticity of the cylindrical lateral surface of the sample used and the convective heat fluxes which originate in the liquid phase; the variability of thermophysical properties with the temperature. In the area affected by the phase change, the most obvious deviations can be mainly attributed to the presence of a phase change temperature range, rather than a single temperature, and to the phenomenon of hysteresis, both a function of the heating/cooling rate. Owing to this phenomenon, the melting temperature and the latent heat of fusion are, respectively, different from the solidification temperature and the latent heat of solidification. Furthermore, also the phase change temperature range and the latent heat vary upon variation of the heating/cooling rate.

Finally, the predictive capacity of the model in the evaluation of the total stored energy calculating the deviations from that determined experimentally was verified. The reduced values of these deviations justify the use of the model to determine the trend of the position of the bi-phase interface as a function of time and the energy stored in the sensible and latent form in the layer.

The maximum total energy stored is recorded in the case in which the attenuation factor is higher and the arguments are almost close, between the two temperature boundary conditions. The reduction of the period gives rise to a reduction of the total stored energy.

Acknowledgements

The work was partially funded by the Spanish government (ENE2015-64117-C5-1-R (MINECO/FEDER), ENE2015-64117-C5-3-R (MINECO/FEDER), and ULLE10-4E-1305). GREA is certified agent TECNIO in the category of technology developers from the Government of Catalonia. The authors would like to thank the Catalan Government for the quality accreditation given to their research group (2014 SGR 123). This project has received funding from the European Commission Seventh Framework Programme (FP/2007-2013) under Grant agreement Nº PIRSES-GA-2013-610692 (INNOSTORAGE) and from European Union's Horizon 2020 research and innovation programme under grant agreement Nº 657466 (INPATH-TES). Alvaro de Gracia would like to thank Ministerio de Economia y Competitividad de España for Grant Juan de la Cierva, FJCI-2014-19940. Julià Coma would like to thank the Departament d'Universitats, Recerca i

Societat de la Informació de la Generalitat de Catalunya for his research fellowship (2016FI_B2 00147). Aran Solé would like to thank Ministerio de Economía y Competitividad de España for Grant Juan de la Cierva, FJCI-2015-25741

Nomenclature

(a)	portion of the layer in phase a
(b)	portion of the layer in phase b
c	specific heat capacity [J/(kg·K)]
D	sample diameter [m]
E	energy stored [J]
f	attenuation factor [-]
F	heat flux [W/m^2]
H	latent heat of fusion [J/kg]
HFM	experimental heat flux [W/m^2]
k	harmonic order [-]
L	thickness of the PCM layer [m]
m	sample mass [kg]
n	number of harmonics [-]
P	period of oscillation [s]
t	time [s]
t*	a particular instant in time [s]
t_1	initial time instant of the phase change [s]
t_2	final time instant of the phase change [s]
T	temperature [K]
TC	experimental temperature [K]
V	volume [m^3]
x	spatial Cartesian coordinates in steady regime [m]
x*	spatial Cartesian coordinates in oscillating regime [m]
X	position of the bi-phase interface [m]

Greek symbols

α	thermal diffusivity [m^2/s]
γ	propagation constant [m^{-1}]
Δ	deviation
Δt	time lag [rad]
ΔV	volume variation [m^3]
Δx	thickness of the subvolume [m]
ζ	argument of the oscillating component of the position of bi-phase interface [rad]
ϑ	generic component of the temperature Fourier series expansion [K]
ϑ_p, ϑ_r	constants of integration [K]

λ	thermal conductivity [W/(m·K)]
ρ	density [kg/m^3]
υ	velocity of the bi-phase interface [m/s]
φ	argument of the temperature oscillation [rad]
ϕ	generic component of the heat flux Fourier series expansion [W/m^2]
χ	generic component of the position of bi-phase interface Fourier series expansion [m]
ψ	argument of the heat flux oscillation [rad]
ω	angular frequency [rad/s]

Subscripts

0	initial time instant of the transient regime
1	face 1
2	face 2
a	phase a
A	sample holder area [m^2]
anal	analytical
b	phase b
bot	referring to the sample bottom surface
cf	referring to the thermal bath that provides the cold fluid
env	referring to the external environment of the test-box
E_T	referring to the total energy stored
exp	experimental
f	final time instant of the transient regime
fus	fusion
H	latent heat stored per unit time
hf	referring to the thermal bath that provides the hot fluid
HFM	referring to the experimental heat flux
j	referring to the j-esimo subvolume of the sample
k	k-th harmonic
l	liquid phase
L	latent heat storage
M	melting
s	solid phase
S	sensible heat storage
sample	referring to the sample holder
sol	solidification
T	total heat storage
TC	referring to the experimental temperature
top	referring to the sample top surface
tot	total sensible heat storage

Symbols

–	mean value
~	oscillating value in the time domain
ˆ	oscillating value in the complex domain
| |	amplitude of an oscillating value
arg	argument of an oscillating value

References

[1] H. Mehling, L. F. Cabeza, Heat and cold storage with PCM, An up to date introduction into basics and applications, Springer, (2008).

[2] J. Bransier, Storage periodique par chaleur latente: aspects fondamentaux lies a la cinetique des transferts, International Journal of Heat and Mass Transfer 22 (1979), pp. 875-883.

[3] J. P. Bardon, E. Vrignaud, D. Delaunay, Etude experimentale de la fusion et de la solidification periodique d'une plaque de paraffine, Revue Générale de Thermique (1979), pp. 212-213.

[4] B. Kalhori, S. Ramadyani, Studies on heat transfer from a vertical cylinder with or without fins embedded in a solid phase change medium, Journal of Heat Transfer 107(1) (1985), pp. 44-51.

[5] C. Belleci, M. Conti, Phase change thermal storage: transient behaviour analysis of a solar receiver/storage module using the enthalpy model, International Journal of Heat and Mass Transfer 36 (1993), pp. 146-156.

[6] C. Belleci, M. Conti, Transient behaviour analysis of latent heat thermal storage module, International Journal of Heat and Mass Transfer 36 (1993), pp. 2157-2163.

[7] C. Belleci, M. Conti, Latent heat thermal storage for solar dynamic power generation, Solar Energy 51 (1993), pp. 169-173.

[8] F. Mathieu-Potvin, L. Gosselin, Thermal shielding of multilayer walls with phase change materials under different transient boundary conditions, International Journal of Thermal Sciences 48 (2009), pp. 1707-1717.

[9] C. K. Halford, R. F. Boehm, Modeling of phase change material peak load shifting, Energy and Buildings 39 (2007), pp. 298-305.

[10] D. A. Neeper, Thermal dynamics of wallboard with latent heat storage, Solar Energy 68(5) (2000), pp. 393-403.

[11] G. Zhou, Y. Yang, H. Xu, Performance of shape-stabilized phase change material wallboard with periodical outside heat flux waves, Applied Energy 88(6) (2011), pp. 2113-2121.

[12] G. Zhou, Y. Yang, X. Wang, J. Cheng, Thermal characteristics of shape-stabilized phase change material wallboard with periodical outside temperature waves, Applied Energy 87(8) (2010), pp. 2666-2672.

[13] N. P. Sharifi, A. A. N. Shaikh, A. R. Sakulich, Application of phase change materials in gypsum boards to meet building energy conservation goals, Energy and Buildings 138 (2017), pp. 455-467.

[14] D. Mazzeo, G. Oliveti, N. Arcuri, Definition of a new set of parameters for the dynamic thermal characterization of PCM layers in the presence of one or more liquid-solid interfaces, Energy and Buildings 141 (2017), pp. 379-396.

[15] V. Jariwala, A.S. Mujumdar, M. E. Weber, The periodic steady state for cyclic energy storage in paraffin wax, The Canadian Journal of Chemical Engineering 65 (1987), pp. 899-906

[16] M. Hasan, A. S. Mujumdar, M. E. Weber, Cyclic melting and freezing, Chemical Engineering Science 46(7) (1991), pp. 1573-1587.

[17] V. R. Voller, P. Felix, C. R. Swaminathan, Cyclic phase change with fluid flow, International Journal of Numerical Methods for Heat & Fluid Flow 6(4) (1996), pp. 57-64.

[18] G. Casano, S. Piva, Experimental and numerical investigation of the steady periodic solid–liquid phase-change heat transfer, International Journal of Heat and Mass Transfer 45 (2002), pp. 4181-4190.

[19] F. Kuznik, J. Virgone, Experimental investigation of wallboard containing phase change material: Data for validation of numerical modeling, Energy and Buildings 41 (2009), pp. 561-570.

[20] S. Savovic, J. Caldwell, Numerical solution of Stefan problem with time dependent boundary conditions by variable space grid method, Thermal Science 13 (2009), pp. 165-174.

[21] M. Ozisik, Heat conduction, Wiley, New York, (1980).

[22] R. Henze, J. Humphrey, Enhanced heat conduction in phase change thermal energy storage devices, International Journal of Heat and Mass Transfer 24 (1981), pp. 450-474.

[23] M. Lachheb, Z. Younsi, H. Naji, M. Karkri, S. B. Nasrallah, Thermal behavior of a hybrid PCM/plaster: A numerical and experimental investigation, Applied Thermal Engineering 111 (2017), pp. 49-59.

[24] H. Ling, C. Chen, H. Qin, S. Wei, J. Lin, N. Li, M. Zhang, N. Yu, Y. Li, Indicators evaluating thermal inertia performance of envelops with phase change material, Energy and Buildings 122 (2016), pp. 175-184.

[25] E. S. Watson, M. J. O'Neill, Joshua J, B. Nathaniel, A differential scanning calorimeter for quantitative differential thermal analysis, Analytical Chemistry 36(7) (1964), pp.1233-1238.

[26] Y. P. Zhang, Jiang Y, Y. Jiang, A simple method, the T-history method, of determining the heat of fusion, specific heat and thermal conductivity of phase-change materials, Measurement Science and Technology 10(3) (1999), pp. 201-205.

[27] A. de Gracia, C. Barreneche, M. M. Farid, L. F. Cabeza, New equipment for testing steady and transient thermal performance of multilayered building envelopes with PCM, Energy and Buildings 43(12) (2011), pp. 3704-3709.
[28] R. Cheng, M. Pomianowski, X. Wang, P. Heiselberg, Y. Zhang, A new method to determine thermophysical properties of PCM-concrete brick, Applied Energy 112 (2013), pp. 988-998.
[29] H. Hu, S. A. Argyropoulos, Mathematical modelling of solidification and melting: a review, Modelling and Simulation in Materials Science and Engineering 4(4) (1996), pp. 371-396.
[30] L.I. Rubinstein, The Stefan Problem, Translations of Mathematical Monographs, vol. 27American, Mathematical Society, Providence, Rhode Island (1971).
[31] J. Crank, Free and Moving Boundary Problems, Oxford: Clarendon, (1984).
[32] H. S. Carslaw, J.C. Jaeger, Conduction of Heat in Solids, second edition, Oxford Science Publications, (1988).
[33] V. Alexiades, A. Solomon, Mathematical Modelling of Melting and Freezing Processes, Hemisphere Publishing Corporation, Washington (1993).
[34] S. Liu, Y. Li, Y. Zhang, Mathematical solutions and numerical models employed for the investigations of Pcm′ phase transformations, Renewable and Sustainable Energy Reviews 33 (2014), pp. 659-674.
[35] D. Mazzeo, G. Oliveti, M. De Simone, N. Arcuri, Analytical model for solidification and melting in a finite PCM in steady periodic regime, International Journal of Heat and Mass Transfer 88 (2015), pp. 844-861.
[36] http://www.puretemp.com. Last access: 25/01/2017
[37] A. Lazaro, C. Peñalosa, A. Solé, G. Diarce, T. Haussmann, M. Fois, B. Zalba, S. Gshwander, L. F. Cabeza, Intercomparative tests on phase change materials characterisation with differential scanning calorimeter, Applied Energy 109 (2013), pp. 415-420.
[38] C. Barreneche, A. Solé, L. Miró, I. Martorell, A. Inés Fernández, Luisa F. Cabeza, Study on differential scanning calorimetry analysis with two operation modes and organic and inorganic phase change material (PCM), Thermochimica Acta 553 (2013), pp. 23-26.
[39] G. Ferrer, C. Barreneche, A. Solé, I. Martorell, L.F. Cabeza, New proposed methodology for specific heat capacity determination of materials for thermal energy storage (TES) by DSC, Journal of Energy Storage 11 (2017), pp. 1-6.
[40] ISO, 1994b International Organization for Standardization, Standard ISO 9869, Thermal insulation: Building elements: In-situ measurement of thermal resistance and thermal transmittance.

[41] D. Mazzeo, G. Oliveti, N. Arcuri, Mapping of the seasonal dynamic properties of building walls in actual periodic conditions and effects produced by solar radiation incident on the outer and inner surfaces of the wall, Applied Thermal Engineering 102 (2016), pp. 1157-1174.
[42] D. Mazzeo, G. Oliveti, Parametric study and approximation of the exact analytical solution of the Stefan problem in a finite PCM layer in a steady periodic regime, International Communications in Heat and Mass Transfer 84 (2017), pp. 49-65.
[43] L. Li, H. Yu, X. Wang, S. Zheng, Thermal analysis of melting and freezing processes of phase change materials (Pcm) based on dynamic DSC test, Energy and Buildings 130 (2016), pp. 388-396.
[44] X. Jin, X. Xu, X. Zhang, Y. Yin, Determination of the PCM melting temperature range using DSC, Thermochimica Acta, 595 (2014), pp. 17-21.
[45] E. Günther, S. Hiebler, H. Mehling, Determination of the heat storage capacity of PCM and PCM-Objects as a function of temperature, in: 10th International Conference on Thermal Energy Storage, ECOSTOCK, (2006).

Table 1 - Constitutive equations of the steady model and of the oscillating model.

	Steady model	Oscillating model
Spatial coordinate	$0 \le x \le L$	$-\bar{\chi}_M \le x^* \le L - \bar{\chi}_M$
Equation of the heat conduction in phase a) and in phase b)	$\frac{d^2\bar{\vartheta}_a(x)}{dx^2} = 0 \qquad 0 \le x \le \bar{\chi}_M$ (Eq. 17)	$\frac{d^2\hat{\vartheta}_a}{dx^{*2}} - \frac{j\omega}{\alpha_a}\hat{\vartheta}_a = 0 \qquad -\bar{\chi}_M \le x^* \le 0$ (Eq. 22)
	$\frac{d^2\bar{\vartheta}_a(x)}{dx^2} = 0 \qquad \bar{\chi}_M \le x \le L$ (Eq. 18)	$\frac{d^2\hat{\vartheta}_b}{dx^{*2}} - \frac{j\omega}{\alpha_b}\hat{\vartheta}_b = 0 \qquad 0 \le x^* \le L - \bar{\chi}_M$ (Eq. 23)
Stefan conditions at the bi-phase interface	$\left[\lambda_a \frac{d\bar{\vartheta}_a}{dx} - \lambda_b \frac{d\bar{\vartheta}_b}{dx}\right]_{x=\bar{\chi}_M} = 0$ (Eq. 19)	$\left[\lambda_a \frac{d\hat{\vartheta}_a}{dx} - \lambda_b \frac{d\hat{\vartheta}_b}{dx}\right]_{x=\hat{\chi}_M} = j\omega\rho H\hat{\chi}_M$ (Eq. 24)
	$\bar{\vartheta}_a(\bar{\chi}_M) = \bar{\vartheta}_b(\bar{\chi}_M) = T_M$ (Eq. 20)	$\hat{\vartheta}_a(\hat{\chi}_M) = \hat{\vartheta}_b(\hat{\chi}_M) = 0$ (Eq. 25)
Boundary conditions	$\bar{\vartheta}_a(0) = \bar{\vartheta}_1 \qquad x = 0$ $\bar{\vartheta}_b(L) = \bar{\vartheta}_2 \qquad x = L$ (Eq. 21)	$\hat{\vartheta}_a(-\bar{\chi}_M) = \hat{\vartheta}_1 \qquad x^* = -\bar{\chi}_M$ $\hat{\vartheta}_b(L - \bar{\chi}_M) = \hat{\vartheta}_2 \qquad x^* = L - \bar{\chi}_M$ (Eq. 26)

Table 2 - Solution of the steady model and of the oscillating model.

	Solution of the steady model	Solution of the oscillating model
Position of the bi-phase interface	$\bar{\chi}_M = \frac{\lambda_a(\bar{\vartheta}_1 - T_M)}{\lambda_a(\bar{\vartheta}_1 - T_M) + \lambda_b(T_M - \bar{\vartheta}_2)} L$ (Eq. 27)	$\frac{\lambda_a \gamma_a}{\sinh[\gamma_a(\bar{\chi}_M + \hat{\chi}_M)]} \hat{\vartheta}_1 + \frac{\lambda_b \gamma_b}{\sinh[\gamma_b(L - \bar{\chi}_M - \hat{\chi}_M)]} \hat{\vartheta}_2 = j\omega\rho H \hat{\chi}_M$ (Eq. 31)
Temperature field in phase (a), in portion in phase change (ab) and in phase (b)	$\bar{\vartheta}_a(x) = T_M + \frac{\bar{\chi}_M - x}{\lambda_a}\bar{\phi}$ $\quad 0 \le x \le \bar{\chi}_M$ (Eq. 28)	$\hat{\vartheta}_a(x^*) = \hat{\vartheta}_1 \left\{ \cosh[\gamma_a(x^* + \bar{\chi}_M)] - \frac{\sinh[\gamma_a(x^* + \bar{\chi}_M)]}{\tanh[\gamma_a(\bar{\chi}_M + \hat{\chi}_M)]} \right\}$ $\quad -\bar{\chi}_M \le x^* \le -\lvert\hat{\chi}_M\rvert$ (Eq. 32)
		$\hat{\vartheta}_{ab}(x^*) = \frac{(L - x^*)\,\hat{\vartheta}_a(x^*) + x\,\hat{\vartheta}_b(x^*)}{L}$ $\quad -\lvert\hat{\chi}_M\rvert \le x^* \le \lvert\hat{\chi}_M\rvert$ (Eq. 33)
	$\bar{\vartheta}_b(x) = T_M - \frac{x - \bar{\chi}_M}{\lambda_b}\bar{\phi}$ $\quad \bar{\chi}_M \le x \le L$ (Eq. 29)	$\hat{\vartheta}_b(x^*) = \hat{\vartheta}_2 \left\{ \cosh[\gamma_b(L - \bar{\chi}_M - x^*)] - \frac{\sinh[\gamma_b(L - \bar{\chi}_M - x^*)]}{\tanh[\gamma_b(L - \bar{\chi}_M - \hat{\chi}_M)]} \right\}$ $\quad \lvert\hat{\chi}_M\rvert \le x^* \le L - \bar{\chi}_M$ (Eq. 34)
Heat flux field in phase (a), in portion in phase change (ab) and in phase (b)	$\bar{\phi}_a = \bar{\phi}_b = \bar{\phi} = \frac{\bar{\vartheta}_1 - \bar{\vartheta}_2}{\frac{\bar{\chi}_M}{\lambda_a} + \frac{L - \bar{\chi}_M}{\lambda_b}}$ (Eq. 30)	$\hat{\phi}_a(x^*) = -\lambda_a \gamma_a \hat{\vartheta}_1 \left\{ \sinh[\gamma_a(x^* + \bar{\chi}_M)] - \frac{\cosh[\gamma_a(x^* + \bar{\chi}_M)]}{\tanh[\gamma_a(\bar{\chi}_M + \hat{\chi}_M)]} \right\}$ $\quad -\bar{\chi}_M \le x^* \le -\lvert\hat{\chi}_M\rvert$ (Eq. 35)
		$\hat{\phi}_{ab}(x^*) = \frac{(L - x)\,\hat{\phi}_a(x^*) + x\,\hat{\phi}_b(x^*)}{L}$ $\quad -\lvert\hat{\chi}_M\rvert \le x^* \le \lvert\hat{\chi}_M\rvert$ (Eq. 36)
		$\hat{\phi}_b(x^*) = \lambda_b \gamma_b \hat{\vartheta}_2 \left\{ \sinh[\gamma_b(L - \bar{\chi}_M - x^*)] - \frac{\cosh[\gamma_b(L - \bar{\chi}_M - x^*)]}{\tanh[\gamma_b(L - \bar{\chi}_M - \hat{\chi}_M)]} \right\}$ $\quad \lvert\hat{\chi}_M\rvert \le x^* \le L - \bar{\chi}_M$ (Eq. 37)

Table 3 - Summary of the DSC results for the two samples of PureTemp23 at 0.5 K/min, 5 K/min and 10 K/min.

0.5 K/min										
Sample	H_{fus}	H_{sol}	T_{fus}	T_{sol}	$T_{onset,fus}$	$T_{offset,fus}$	$T_{onset,sol}$	$T_{offset,sol}$	ΔT_{fus}	ΔT_{sol}
	(kJ/kg)	(kJ/kg)	(ºC)	(ºC)	(ºC)	(ºC)	(ºC)	(ºC)	(ºC)	(ºC)
1	215.61	219.10	24.57	21.31	23.01	25.45	20.74	20.28	2.44	0.46
2	215.87	214.09	24.46	21.10	22.72	25.33	20.57	20.14	2.61	0.43
mean	215.74	216.60	24.52	21.21	22.87	25.39	20.66	20.21	2.53	0.44
sd	0.18	3.54	0.08	0.15	0.21	0.08	0.12	0.10	0.12	0.02
5 K/min										
Sample	H_{fus}	H_{sol}	T_{fus}	T_{sol}	$T_{onset,fus}$	$T_{offset,fus}$	$T_{onset,sol}$	$T_{offset,sol}$	ΔT_{fus}	ΔT_{sol}
	(kJ/kg)	(kJ/kg)	(ºC)	(ºC)	(ºC)	(ºC)	(ºC)	(ºC)	(ºC)	(ºC)
1	198.65	200.62	24.88	18.17	21.79	28.74	18.23	14.75	6.95	3.48
2	200.51	199.65	24.89	18.39	21.77	28.67	18.45	14.94	6.90	3.51
mean	199.58	200.14	24.89	18.28	21.78	28.71	18.34	14.85	6.93	3.50
sd	1.32	0.69	0.01	0.16	0.01	0.05	0.16	0.13	0.04	0.02
10 K/min										
Sample	H_{fus}	H_{sol}	T_{fus}	T_{sol}	$T_{onset,fus}$	$T_{offset,fus}$	$T_{onset,sol}$	$T_{offset,sol}$	ΔT_{fus}	ΔT_{sol}
	(kJ/kg)	(kJ/kg)	(ºC)	(ºC)	(ºC)	(ºC)	(ºC)	(ºC)	(ºC)	(ºC)
1	200.05	200.63	25.91	16.80	21.91	31.79	18.06	11.61	9.88	6.45
2	195.41	195.48	26.23	16.77	21.97	32.08	17.82	11.19	10.11	6.63
mean	197.73	198.06	26.07	16.79	21.94	31.94	17.94	11.40	10.00	6.54
sd	3.28	3.64	0.23	0.02	0.04	0.21	0.17	0.30	0.16	0.13

Table 4 - Measured values of temperatures T_{top} and T_{bot} on the two faces of the sample at final instant t_f and initial instant t_0 of the thermal transient, of steady heat fluxes F_f at final instant t_f, of the stored sensible energy E_S, of the thermal conductivity λ and of the specific heat capacity c, in the two experimental tests with the sample entirely in solid and in liquid phase.

	$T_{top,f}$ (°C)	$T_{bot,f}$ (°C)	$T_{top,0}$ (°C)	$T_{bot,0}$ (°C)	F_f (W/m^2)	E_S (J/m^2)	λ (W/m·K)	c (J/kg·K)
Solid phase *s*	14.09	4.33	0.33	0.12	32	3166	0.233	1504.8
Liquid phase *l*	57.60	35.80	28.56	28.58	49	8690	0.160	2047.9

Table 5 - Sensible energy stored in the solid phase and in the liquid phase by each subvolume and by the entire layer, total sensible energy stored and total energy stored.

Subvolume j	1	2	3	4	5	Tot	$E_{S,tot}$ (J)	E_T (J)
$E_{S,s}$ (J)	99.0	188.2	210.2	209.4	91.0	797.8	1088.5	52867
$E_{S,l}$ (J)	40.5	87.9	74.0	58.6	29.6	290.7		

Table 6 - Thermophysical properties of the PureTemp23 PCM sample used in the device.

ρ_s (kg/m^3)	ρ_l (kg/m^3)	ρ (kg/m^3)	λ_s (W/m·K)	λ_l (W/m·K)	c_s (J/kg·K)	c_l (J/kg·K)	T_M (°C)	H (kJ/kg)
865.25	831	848.13	0.233	0.160	1504.8	2047.9	22.47	221.18

Table 7 - Tests in a sinusoidal and non-sinusoidal regime: order k and period P of the harmonics used in the Fourier series expansion, mean steady value $|\tilde{\vartheta}_1|$ and $|\tilde{\vartheta}_2|$, amplitude $|\tilde{\vartheta}_1|$ and $|\tilde{\vartheta}_2|$, and argument $arg(\tilde{\vartheta}_1)$ and $arg(\tilde{\vartheta}_2)$ of the two boundary conditions, attenuation factor f and time lag Δt between the two boundary conditions.

TEST IN SINUSOIDAL PERIODIC REGIME										
			Top surface temperature			Bottom surface temperature				
TEST	k	P (hours)	$\bar{\vartheta}_1$ (°C)	$\lvert\tilde{\vartheta}_1\rvert$ (°C)	$\arg(\tilde{\vartheta}_1)$ (rad)	$\bar{\vartheta}_2$ (°C)	$\lvert\tilde{\vartheta}_2\rvert$ (°C)	$\arg(\tilde{\vartheta}_2)$ (rad)	f (-)	Δt (rad)
1	1	24	33.000	9.547	0.950	12.260	4.379	7.115	0.459	6.166
2	1	24	33.910	9.985	1.060	12.650	1.034	6.265	0.104	5.205
4	1	12	33.900	8.278	-0.697	12.310	3.389	5.570	0.409	6.267
5	1	24	34.542	10.640	2.647	12.717	3.188	4.155	0.300	1.508
TEST IN NON SINUSOIDAL PERIODIC REGIME										
			Top surface temperature			Bottom surface temperature				
TEST	k	P (hours)	$\bar{\vartheta}_1$ (°C)	$\lvert\tilde{\vartheta}_1\rvert$ (°C)	$\arg(\tilde{\vartheta}_1)$ (rad)	$\bar{\vartheta}_2$ (°C)	$\lvert\tilde{\vartheta}_2\rvert$ (°C)	$\arg(\tilde{\vartheta}_2)$ (rad)	f (-)	Δt (rad)
3	1	24	34.092	5.650	-1.366	12.493	1.840	-0.814	0.326	0.552
	2	12		2.766	1.454		0.900	3.005	0.326	1.551
	3	8		3.077	2.184		1.032	4.973	0.335	2.789
	4	6		1.330	0.245		0.372	3.649	0.279	3.404
	5	4.8		0.753	-1.527		0.277	2.273	0.368	3.800

Table 8 - For the different tests, heat flux steady mean value measured on the top surface $\overline{HFM_{top}}$ and on the bottom surface $\overline{HFM_{bot}}$, absolute $\Delta_{\overline{HFM}}$ and percentage Δ% deviation, heat flux steady mean value calculated analytically $\bar{\phi}$ and percentage deviations Δ_{top}% and Δ_{bot}% between the two measured heat fluxes and the analytical one.

	TEST 1	TEST 2	TEST 4	TEST 5	TEST 3
$\overline{\mathrm{HFM_{top}}}$ $(\mathrm{W/m^2})$	53.40	54.99	58.55	57.39	55.54
$\overline{\mathrm{HFM_{bot}}}$ $(\mathrm{W/m^2})$	60.07	59.95	59.15	61.51	61.31
$\Delta_{\overline{\mathrm{HFM}}}$ $(\mathrm{W/m^2})$	-6.67	-4.97	-0.59	-4.11	-5.77
Δ%	-12.49	-9.04	-1.01	-7.17	-10.38
$\bar{\phi}$ $(\mathrm{W/m^2})$	57.12	57.89	58.99	59.09	58.81
Δ_{top}%	-6.51	-5.02	-0.74	-2.88	-5.57
Δ_{bot}%	5.17	3.57	0.27	4.08	4.24

Table 9 - For the different tests, experimental and analytical value of the total stored energy and percentage deviation.

	TEST 1	TEST 2	TEST 4	TEST 5	TEST 3
$\mathrm{E_{T,exp}}$ (kJ)	8.90	5.80	4.22	6.13	4.66
$\mathrm{E_{T,anal}}$ (kJ)	8.67	5.81	4.11	5.68	5.51
$\Delta_{\mathrm{E_T}}$ %	-2.65	0.17	-2.68	-7.92	15.43

Table 10 - For the different tests, sensible and latent stored energy.

	TEST 1	TEST 2	TEST 4	TEST 5	TEST 3
$\mathrm{E_{S,anal}}$ (kJ)	8.31	5.49	3.91	5.39	5.17
$\mathrm{E_{L,anal}}$ (kJ)	0.56	0.38	0.25	0.41	0.36

PureTemp 23 Technical Information

PureTemp 23 is a USDA Certified Biobased product

Appearance	Clear liquid, waxy solid
Melting point	23 °C
Heat storage capacity	201 J/g
Thermal conductivity (liquid)	0.15 W/m°C
Thermal conductivity (solid)	0.25 W/m°C
Density (liquid)	0.83 g/ml
Density (solid)	0.91 g/ml
Specific heat (liquid)	1.99 J/g°C
Specific heat (solid)	1.84 J/g°C

Typical physical properties are listed in the table above.

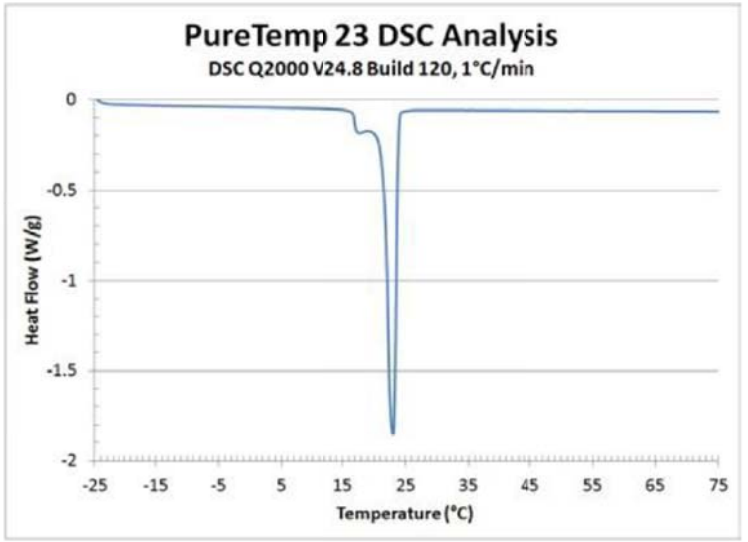

Figure 1 - PCM PureTemp23, thermophysical properties and DSC curve with a heating rate of 1°C/min [36].

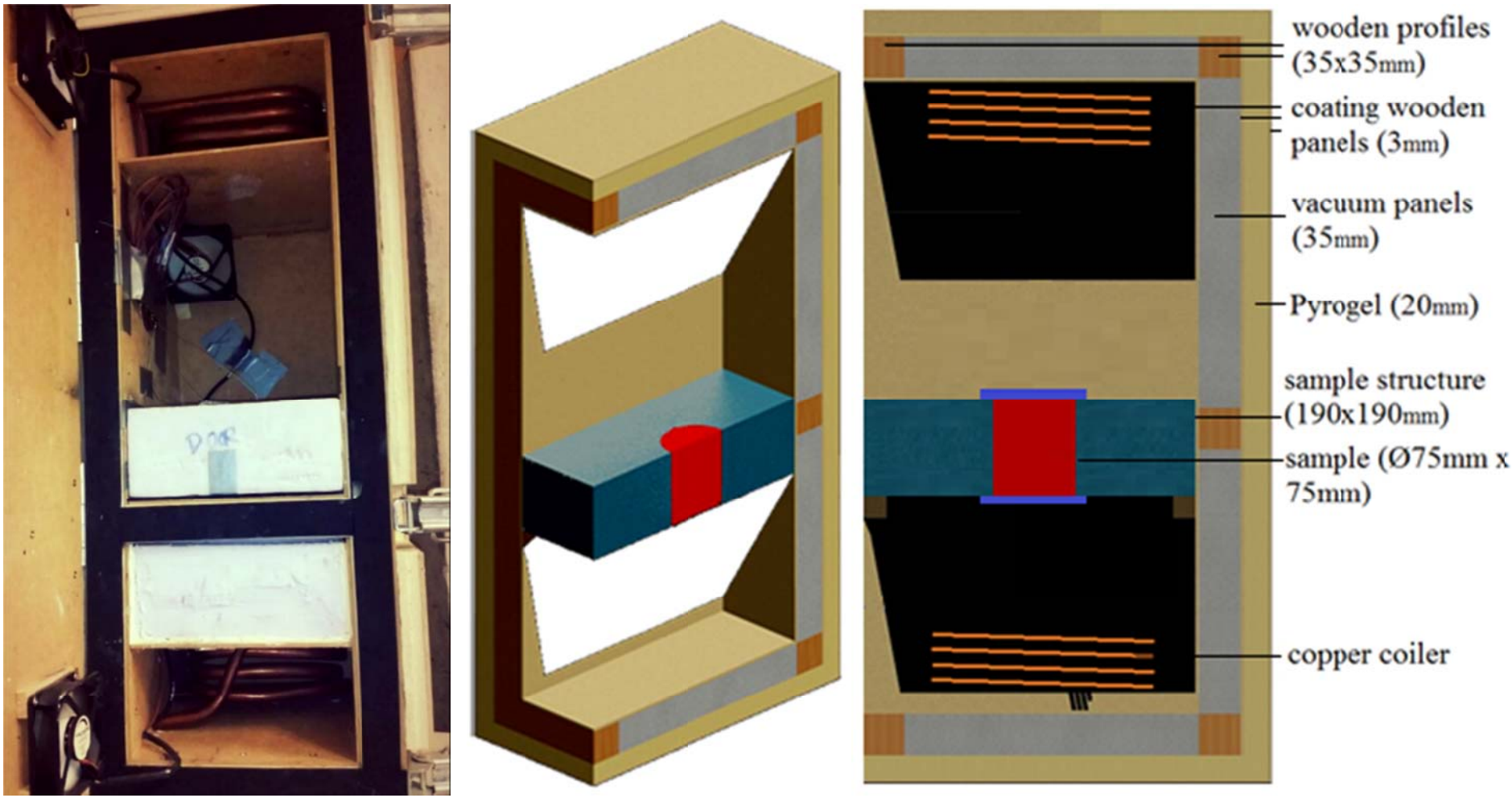

Figure 2 - Sections of the test-box scheme design.

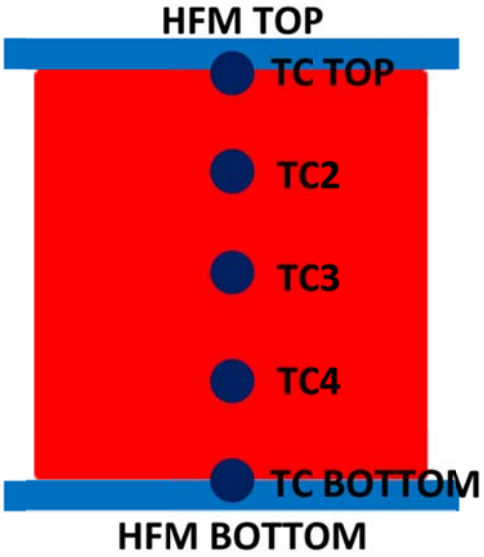

Figure 3 - Position of the thermocouples TC and the heat flux meters HFM in the cylindrical PCM sample.

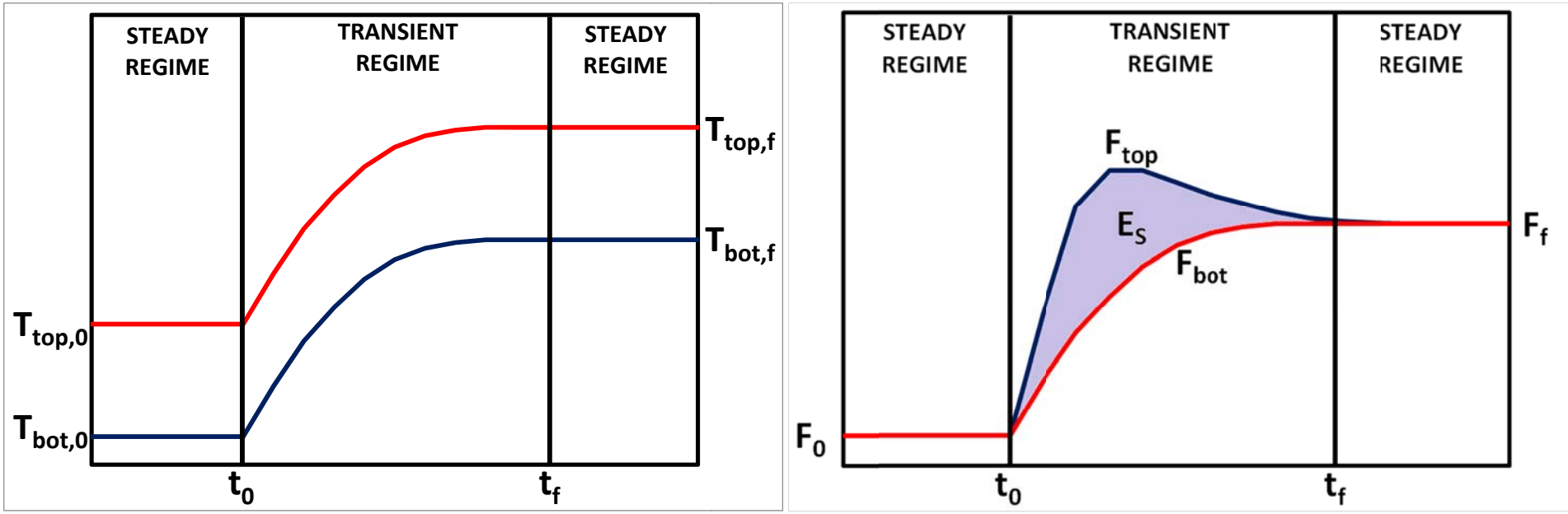

Figure 4 - Schematization of temperature trends T_{top} and T_{bot}, on the left, and of surface heat fluxes trends F_{top} and F_{bot} and of the stored sensible energy E_S, on the right, during the thermal transient between an initial steady state and a final steady state, to be used for the determination of the thermal conductivity and specific heat in the two phases.

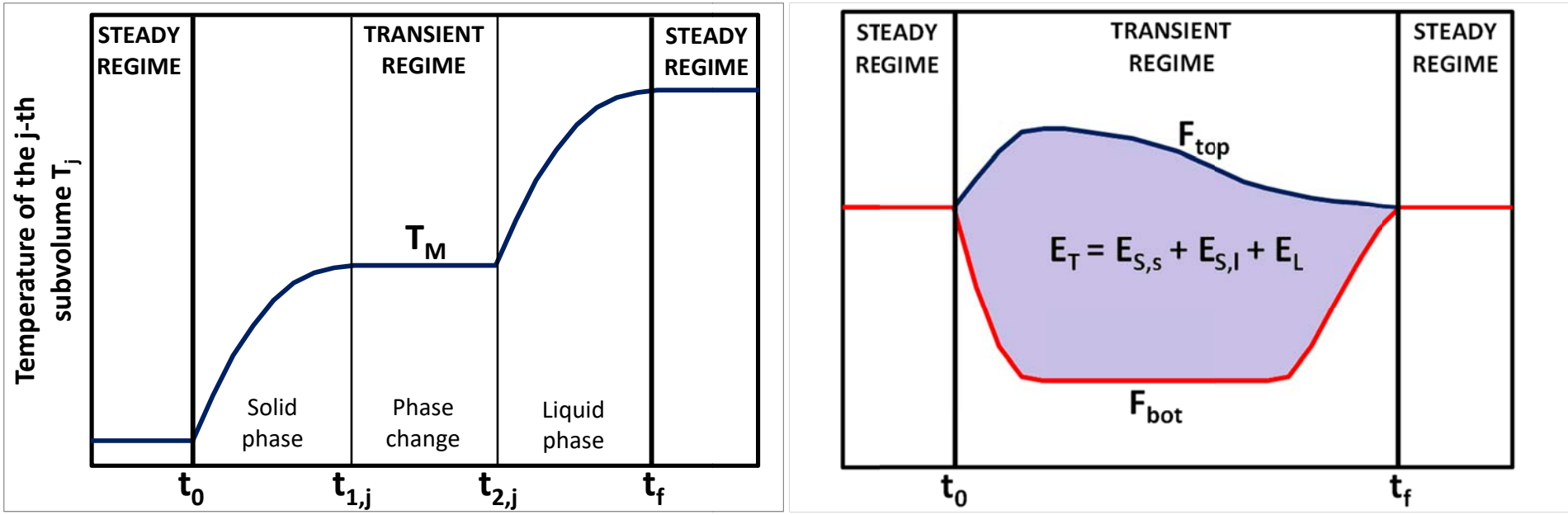

Figure 4 - Schematization of temperature trends T_{top} and T_{bot}, on the left, and of surface heat fluxes trends F_{top} and F_{bot} and of the stored sensible energy E_S, on the right, during the thermal transient between an initial steady state and a final steady state, to be used for the determination of the thermal conductivity and specific heat in the two phases.

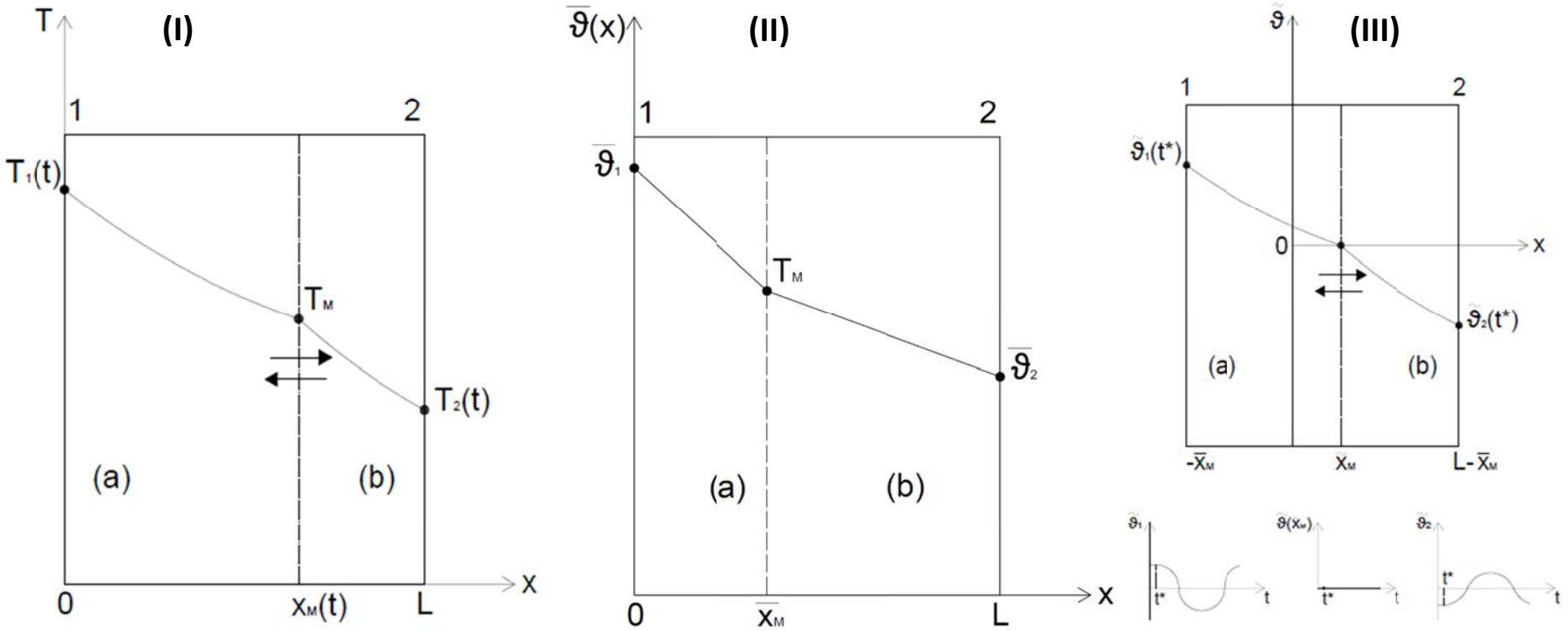

Figure 6 - Reference system of the bi-phase interface position, boundary conditions and temperature trend in the liquid phase (a) and in the solid phase (b) in the PCM layer. (I) steady component + oscillating component; (II) steady component; (III) oscillating component.

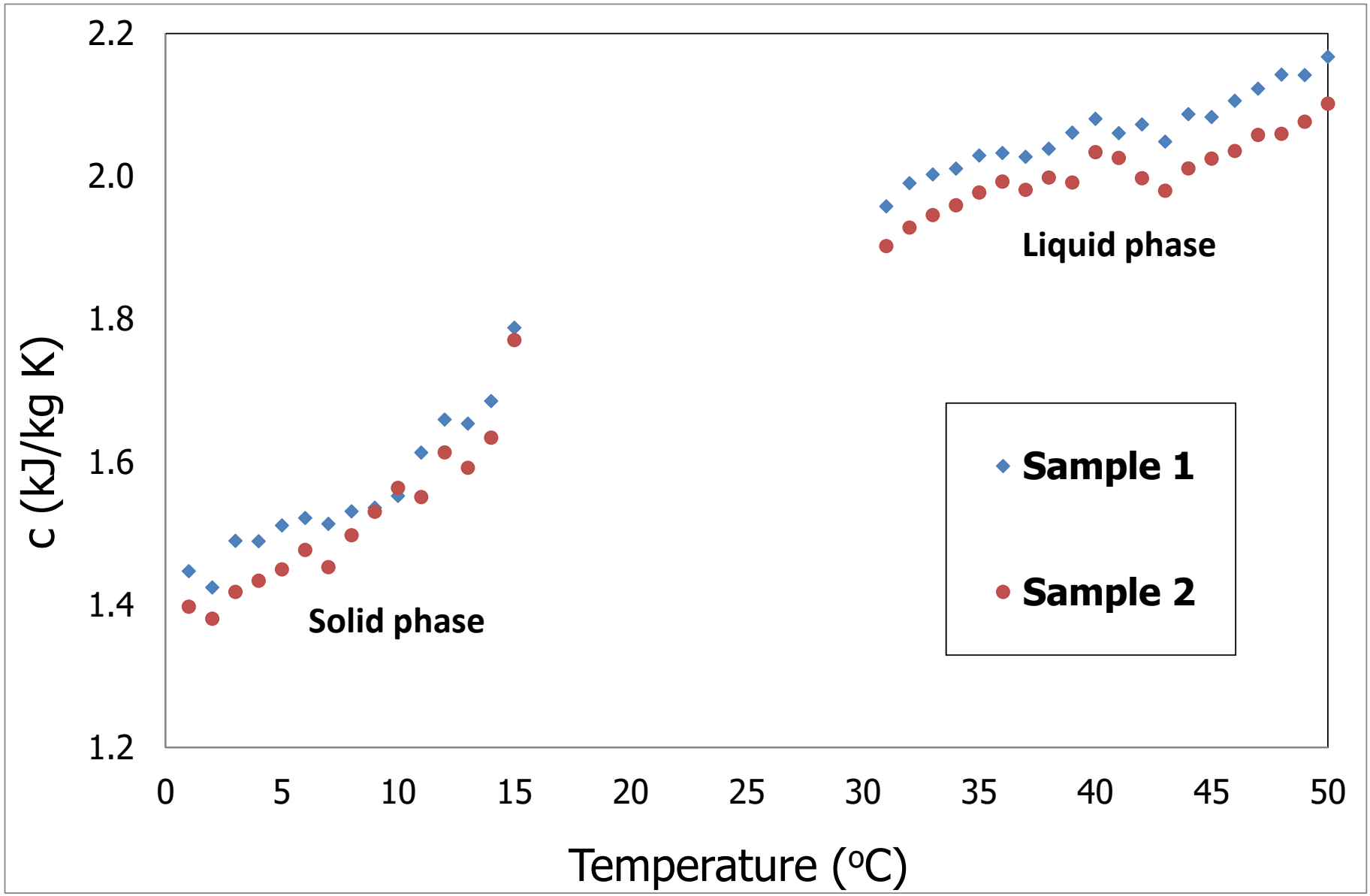

Figure 7 - Specific heat capacity as a function of the temperature for the solid phase and liquid phase of the two samples of Pure Temp 23.

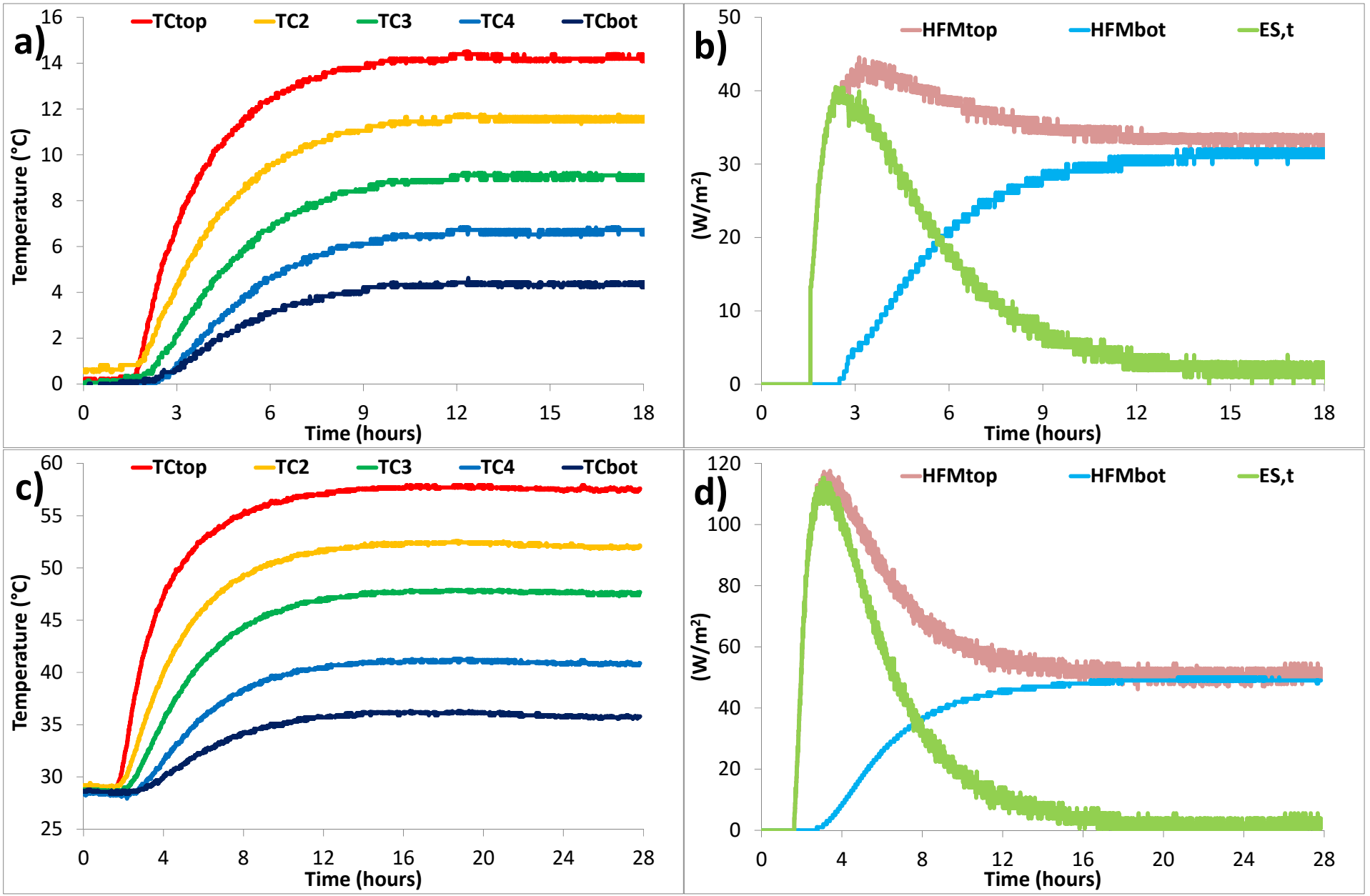

Figure 8 - Trends of the temperatures TC at different heights, of the surface heat fluxes HFM and of the sensible energy stored per unit time $E_{S,t}$. (a) and (b) solid phase; (c) and (d) liquid phase.

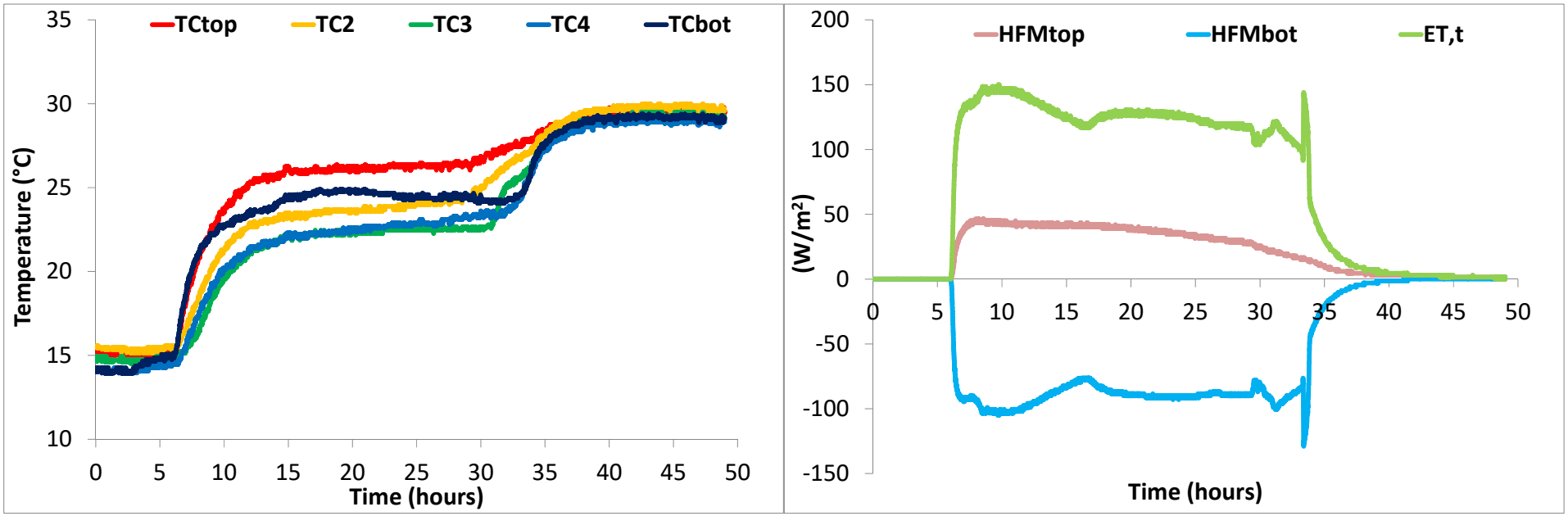

Figure 9 – (a) Temperature trends at the different heights; (b) trends of the surface heat fluxes and of the sensible energy stored per unit time.

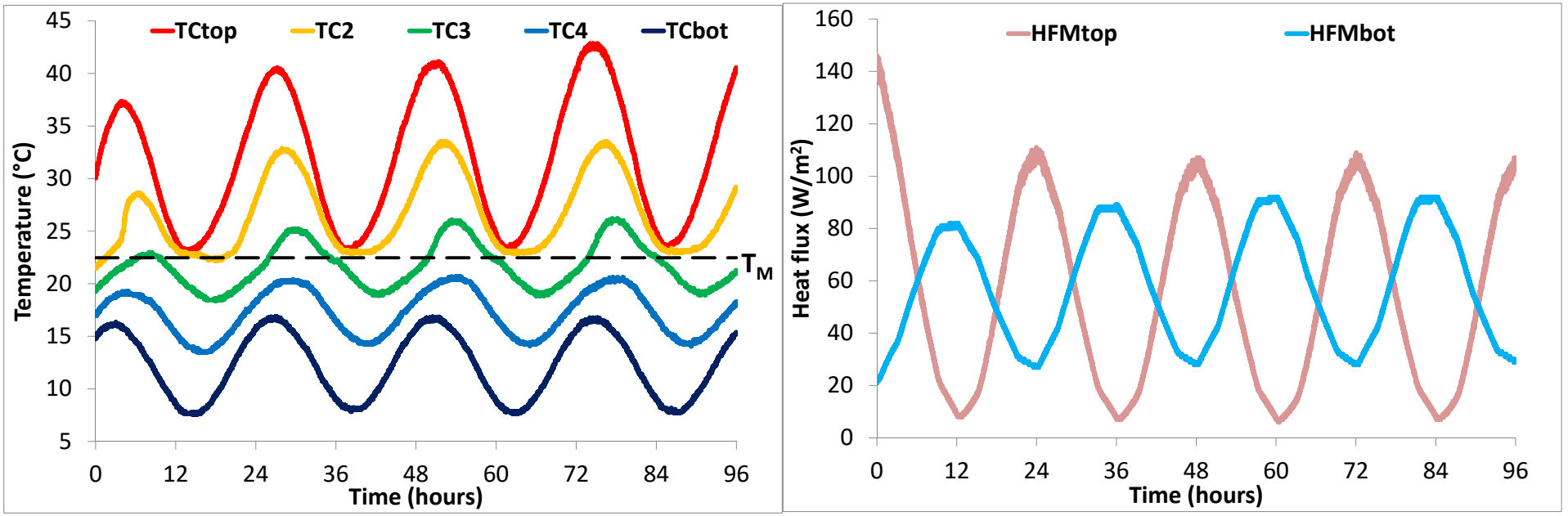

Figure 10 - Thermal transient during TEST 1 until attainment of the steady periodic regime of temperatures at different heights and of the surface heat fluxes.

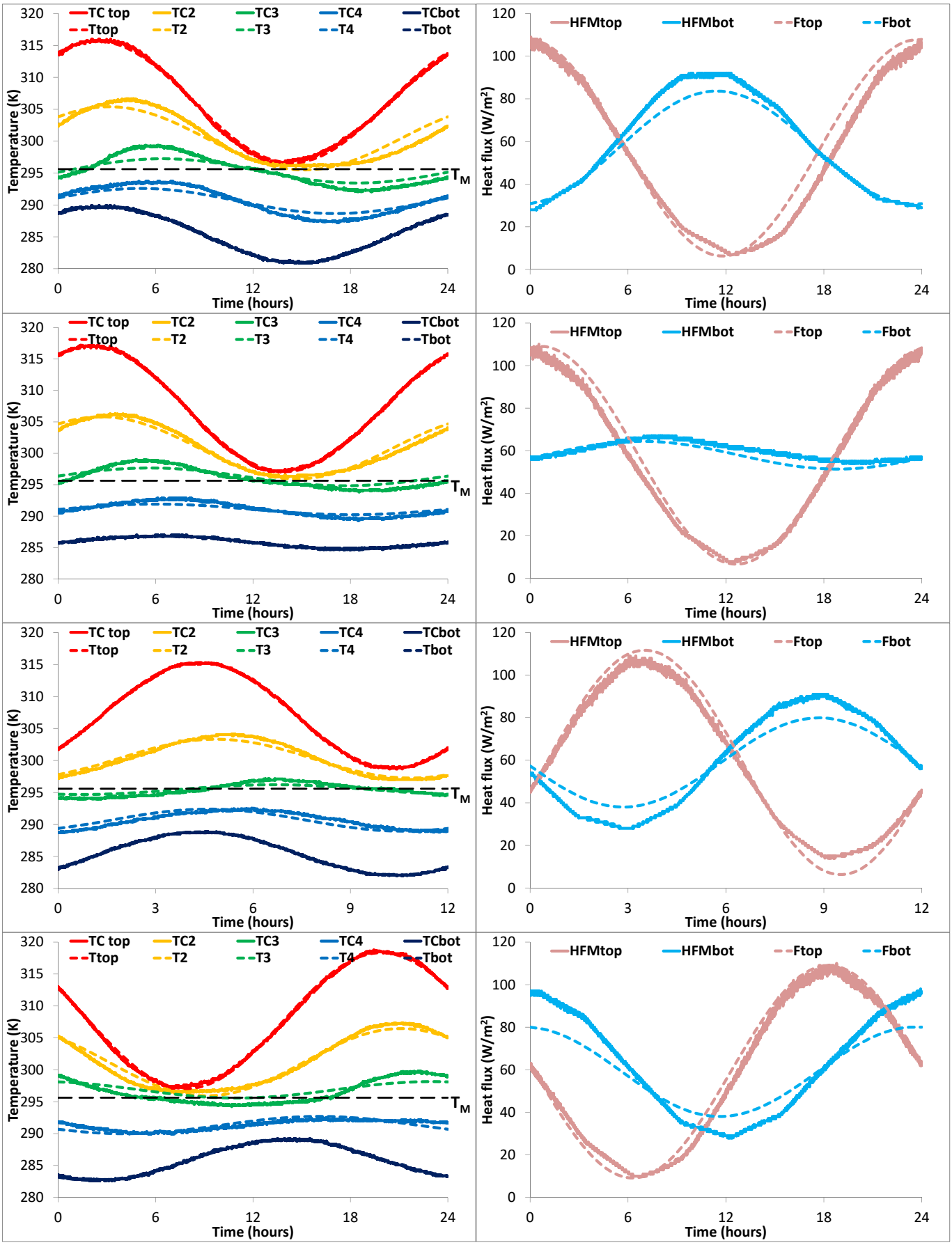

Figure 11 - Comparison between the measured (TC and HFM) and calculated (T and F) temperature trends at different heights, on the left, and of the surface heat fluxes, on the right, in the case of test in a sinusoidal periodic regime. From the top to the bottom in the order: TEST1, TEST2, TEST4 and TEST5.

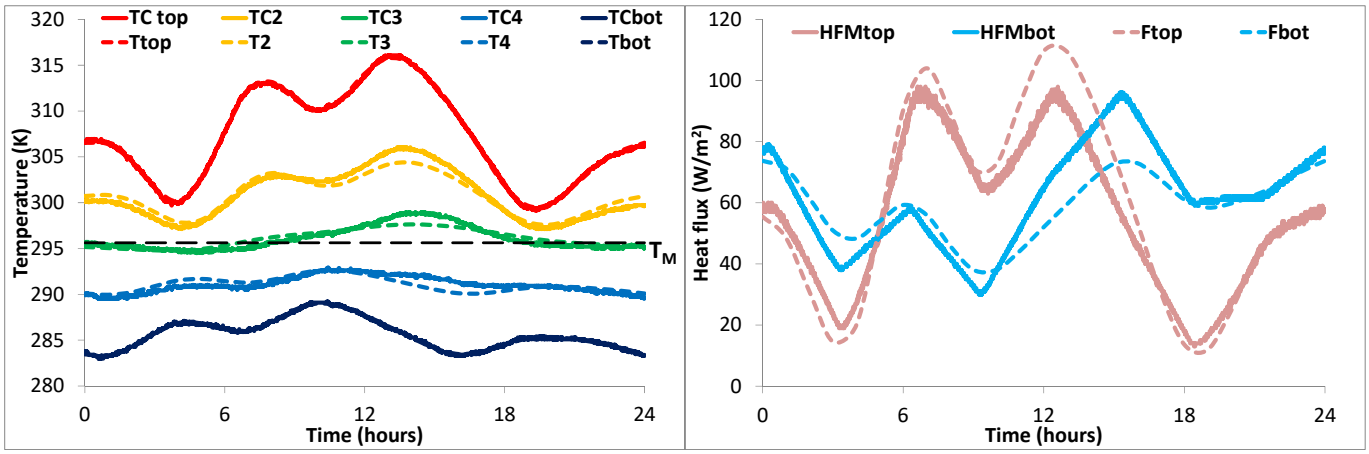

Figure 12 - Comparison between the measured (TC and HFM) and calculated (T and F) temperature trends at different heights, on the left, and of the surface heat fluxes, on the right, in the case of test in a non-sinusoidal periodic regime.

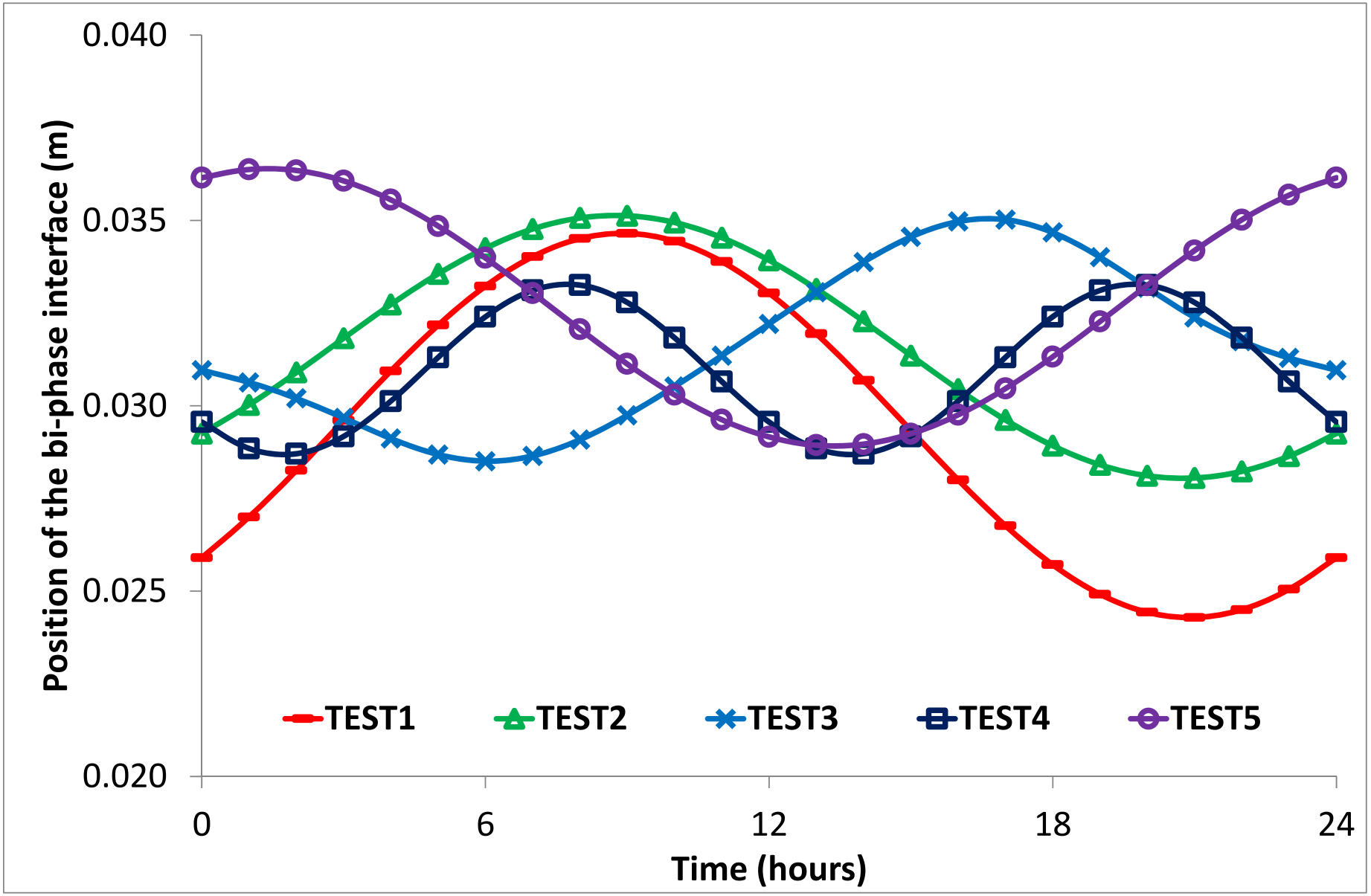

Figure 13 - For the different tests, trend of the position of the bi-phase interface as a function of time.